Lightest flavor-singlet *qqq* baryons as witnesses to color

Jonathan Estévez and Felipe J. Llanes-Estrada

Universidad Complutense de Madrid, Departamento de Física Teórica and IPARCOS,
Plaza de las Ciencias 1, 28040 Madrid, Spain

Víctor Martínez-Fernández

National Centre for Nuclear Research (NCBJ), Ludwika Pasteura 7, 02-093, Warsaw, Poland

Álvaro Pastor-Gutiérrez

Institut für Theoretische Physik, Universität Heidelberg, Philosophenweg 16, 69120 Heidelberg, Germany

We present a new computation in a field-theoretical model of Coulomb-gauge QCD of the first radial and angular excitations of a *qqq* system in an $SU(3)$ flavor-singlet state, Λ_S. The traditional motivation for the study is that the absence of flavor singlets in the lowest-lying spectrum is a direct consequence of the color degree of freedom. [The calculation is tested with decuplet baryons $\Delta(1232)$ and $\Omega(1672)$.] We also analyze decay branching fractions of the flavor-singlet baryon for various masses with the simplest effective Lagrangians.

I. INTRODUCTION

A. Color confinement and the three-quark baryon singlet Λ_S

When one examines the empirical basis for "confinement," it is easy to come across studies of "quark confinement" since fractional charges are a feasible target for searches in Millikan-type experiments [1] or at high-energy accelerators [2]. However, the theoretical concept that makes sense is rather "color confinement" (for which the experimental evidence is not so unquestionable [3], since color leaks by neutral gluons have, surprisingly, not been purposefully constrained).

Though color is not a useful quantum number for hadron classification, as we believe they are all color singlets, there are effects due to color in hadron spectroscopy. For example, the predicted Regge trajectories of meson and baryon resonances have different slopes, which can be traced to the $4/3$ versus $2/3$ color factors in gluon exchange between qq and $q\bar{q}$ pairs. Another example is the $\pi_0 \to \gamma\gamma$ decay, sensible to N_c.

This article is driven by our curiosity about the following classic statement at the root of the quark model and QCD, for which we collect extant evidence from experiment

and theoretical computations, including new ones. A *qqq* baryon configuration must be a color singlet, if color is confined; this is achieved by the antisymmetric $\sqrt{\frac{1}{3!}}\epsilon_{ijk}B_i^\dagger B_j^\dagger B_k^\dagger|\Omega\rangle$ color wave function (the quark creation operators $B^\dagger$ and color vacuum state $|\Omega\rangle$ will be modeled in BCS approximation in Sec. IV below).

The antisymmetry of the color wave function forces the visible degrees of freedom (spin, orbital angular momentum, quark flavor, and eventually, radial-like excitations), due to the fermionic nature of spin-$\frac{1}{2}$ quarks, to be in a totally symmetric wave function, quite unlike nucleon wave functions in nuclei or electron wave functions in atomic, molecular, or solid-state physics.

Chromomagnetic interactions are large in QCD, so one expects (as is typical in hadron physics) that states with lower total angular momentum J have smaller masses. The energy of *qqq* baryon configurations should be smallest if the spatial degrees of freedom could all be in an s wave, and also in the lowest radially excited state, that is,

$$\psi_{\text{spatial}} = \prod_{i=1}^{3} Y_0^0(\hat{\mathbf{k}}_i)R_0(|\mathbf{k}_i|), \qquad \sum_{i=1}^{3}\mathbf{k}_i = \mathbf{0}. \quad (1)$$

Since this is a completely symmetric wave function, the remaining product of spin and flavor degrees of freedom must also be in a totally symmetric configuration. This means that the lowest two multiplets in the baryon spectrum are Gell-Mann's flavor octet and decuplet [4,5] that combine mixed-symmetry flavor and spin wave

functions (the octet) and completely symmetric spin and flavor wave functions (the decuplet).

The empirical consequence of this quantum wave function organization is the absence of a qqq flavor singlet in the lowest-lying spectrum; its antisymmetry would require an antisymmetric spin wave function for the spin-flavor product to be symmetric. As it is not possible to antisymmetrize three quarks with only 2 degrees of freedom (one would be repeated), a flavor singlet with the color degree of freedom requires a spatial-wave-function excitation (so that part can separately be antisymmetrized). This excitation raises the flavor-singlet mass. Schematically,

$$\psi^A_{qqq} = \psi^A_{color} \otimes \psi^A_{flavor} \otimes (\psi_{spin} \otimes \psi_{radial} \otimes \psi_{orbitalL})^A, \quad (2)$$

where the A superindex indicates each of the parts that need to separately be antisymmetric. There are several ways of achieving antisymmetry of the last parenthesis, and the resulting lowest-energy qqq wave functions are explicitly constructed in Sec. II below.

It is therefore of theoretical interest to be able to identify a state which coincides, in all or in a good part, with the three-quark antisymmetric flavor-singlet configuration. This is to be found within the (uds) Λ hyperon spectrum that contains Λ_S, the possible singlets.

To discuss the lightest of those flavor-singlet states, in this study we consider baryons with just one quantum of excitation.

B. Excited Λ spectrum

The ground-state Λ hyperon is well assigned to Gell-Mann's octet: Therefore, and as expected, the search for a singlet needs to concentrate on excited states. There are two prominent low-energy Λ excitations, the $J^\pi = \frac{3}{2}^- \Lambda(1520)$ and the $J^\pi = \frac{1}{2}^- \Lambda(1405)/\Lambda(1380)$ double system, both with negative parity [6]. But as we will show later in Sec. II,

one expects a qqq singlet configuration with only one quantum of excitation in the $\frac{1}{2}^+$ sector, so we briefly comment on all three channels here.

1. $J^\pi = \frac{1}{2}^-$

The first apparent excitation of the Λ is the S-wave $\Lambda(1405)$ system, widely believed to be formed by two particles of equal quantum numbers [7,8] (see, more recently, [9]) mixed from a singlet and two octets with $J^\pi = \frac{1}{2}^-$. In that classic work, the limit of exact $SU(3)$ symmetry reveals that one of the particle poles, at 1450 MeV, corresponds to a singlet. This pole is generated by the dynamics of the $N - K$ interaction [two octets can yield a singlet irreducible representation of $SU(3)$]. Upon breaking $SU(3)$, however, it mixes with the Λ_8 octets and goes down in mass to 1390 MeV.

In lattice gauge theory, a state compatible with this $\Lambda(1405)$ was found to give a strong signal with a flavor-singlet interpolating operator [10], making it the lightest solid candidate to belong to the Λ_S singlet family, but how much of the genuine qqq singlet is therein (and how much corresponds to molecularlike configurations, $N\bar{K}$, for example) remained unclear. The answer to this question, as given by [11], is that, at physical pion masses, the state is mostly an antikaon-nucleon bound molecule (as earlier discussed for a long time). Unfortunately, because the interpolator used is an ideally mixed uds configuration, both singlet and octet can contribute to this lattice signal, so the flavor representation or mixing (under scrutiny here) is not extracted. Interestingly, for unphysical pion masses of order the kaon mass or higher, the lattice state becomes an intrinsic (presumably qqq) state, but then its mass is in the 1.7–1.8 GeV range, 400 MeV above the data.

Next, in one of the Graz quark-model computations [12], the Goldstone boson exchange (GBE) model (in which quarks exchange pions instead of gluons), the computed

TABLE I.   The lattice QCD data from [13,14] show a spectrum of Λ resonances at substantially larger mass than the experimental states. This is natural taking into account that the pion mass m_π is taken in the interval 300–700 MeV in the lattice simulations (in effect closing the decay phase space) corrected by a linear extrapolation $M_\Lambda \propto a + bm_\pi^2$ to the physical 138 MeV mass. Thus, our Coulomb-QCD model computation of pure qqq states (selected in a flavor-singlet configuration) is more comparable to this lattice calculation than directly to the experimental spectrum. Our restriction of the flavor to a singlet is likely raising the mass, as can be seen when comparing to other theoretical approaches. All masses are rounded off to 5 MeV.

Experimental		Mixed uds configurations			Singlet configuration
Λ candidates	Lattice	Graz models	Bonn model [15] ([16])	Dyson-Schwinger [17]	Coulomb-gauge model (this work)
$\Lambda(1380 + 1405)^{\frac{1}{2}^-}$	1600 [10]	1555 (GBE)	1620 (1511)	1315	
$\Lambda(1670)^{\frac{1}{2}^-}$	1450 [11]	1630 (OGE)	1695 (1635)	(1580*)	1800 ± 200
$\Lambda(1800)^{\frac{1}{2}^-}$			1830 (1774)		
$\Lambda(1520)^{\frac{3}{2}^-}$	1950	1555 (GBE)	1595 (1500)		1700 ± 200
$\Lambda(1690)^{\frac{3}{2}^-}$	1750 [18]	1630 (OGE)	1710 (1650)		
$\Lambda(1600)^{\frac{1}{2}^+}$	1900 [19]	1625 (GBE)	1590 (1665)	1475	2400 ± 150
$\Lambda(1810)^{\frac{1}{2}^+}$		1745 (OGE)	1790 (1750)	(1580*)	

mass fits the assignment of $\Lambda(1405) \to \Lambda_S$ (see Table I), but this model is less widely accepted to represent quark interactions than their one gluon exchange (OGE) model that yields a higher mass: This is in agreement with the lattice result of [10], but now too high with respect to the experimental datum.

There are two further relatively clear $\frac{1}{2}^-$ excitations at 1670 and 1800 MeV, completing the picture of a singlet and two octets from the meson-nucleon molecule picture and also quark-model expectations. It is a fair question to ask how is the qqq flavor singlet distributed among these three states, if at all: The lowest states seem very much influenced by the baryon-meson configuration, and the higher ones have traditionally been assigned to nonsinglet multiplets.

2. $J^\pi = \frac{3}{2}^-$

The second well-known Λ excitation appears at slightly higher energy above the KN threshold, the $\Lambda(1520)$, which is a very prominent peak [20] with $J^\pi = \frac{3}{2}^-$, decaying to both $\Sigma\pi$ and $N\bar{K}$ channels. The lattice computation (typical of what would be a pure qqq state) yields a mass of 1950 MeV in this channel, remarkably higher. The Graz quark models are closer to the experimental mass.

This is a general pattern: Lattice gauge theory data [13,14] show a Λ spectrum that is systematically too high with respect to the experimental one. A likely reason is that the higher than physical pion mass employed in lattice simulations decouples the meson-nucleon channel, returning the energy of the would-be three-quark core. In this way, our own qqq computation in the North Carolina State University (NCState) Coulomb-gauge model presented below in Sec. IV, should more naturally be compared to lattice data than to experimental data. This is shown in Table I.

There is a second resonance with these quantum numbers, $\Lambda(1690)$, that is usually assigned to a baryon octet [21]. It is this resonance that was possibly being picked up by early lattice studies, due to a poor choice of interpolating field. This was resolved by an improved choice with built-in parity and flavor structure by Meinel and Rendon [18]: for pion masses around 300 MeV, they find $\Lambda\frac{3}{2}^-$ masses around 1750 MeV, suggesting how much the 1520 resonance goes up upon closing its decay channels.

3. $J^\pi = \frac{1}{2}^+$

If the singlet is searched for with the same J^π quantum numbers as the ground-state Λ, the internal qqq structure needs to be assigned a radial-like excitation.

There are two experimentally known resonances, $\Lambda(1600)$ and $\Lambda(1810)$, though this second one apparently is not strictly needed to improve the global fit quality [22]. It is however the one that the Graz group considers the most likely singlet candidate [12] in view of their calculations.

The Dyson-Schwinger computation [17] predicts a uds excitation with $\frac{1}{2}^+$ around 1475 MeV, though the authors believe that model dependence is dragging it downward: If they opt for artificially weakening their kernel interaction, by less than 10%, they bring it up to 1580 MeV, in line with other qqq approaches. This is marked with an asterisk in Table I.

Several other aspects of the table merit comment. We quote two different instanton-interacting Bonn quark-model computations from [15,16]. They differ in that the latter employs a flavor-independent kernel, whereas the former, a later computation, introduces a flavor dependence to improve agreement with the data. This is achieved, but then disagreement with lattice data (that should better represent the qqq configuration) arises.

C. Flavor structure

As $SU(3)$ symmetry is not exact, octet-singlet flavor mixing (and eventually, even with higher representations) is expected to happen. Of mesons we know, for example, that the ω is purely $u\bar{u} + d\bar{d}$, while the ϕ is almost entirely $s\bar{s}$ (ideal mixing), and the pseudoscalar η, η' pair is in a differently mixed configuration, though not purely octet singlet; ground-state baryons are, however, widely believed to be in a rather good octet configuration. Remarkably, the Gell-Mann-Okubo formulas for the octet $\frac{1}{2}^+$ baryons are accurate [21] to $O(15 \text{ MeV}) \sim 1\%$–$2\%$ despite the possible mixing. The mixing seems to be small, and because its dependence in the controlling $\sin\theta_{1-8}$ is quadratic, the angle is difficult to extract with precision.

Turning to the excited states with which we here deal, assigning the $\frac{3}{2}^-$ $\Lambda(1520)$ to be a pure flavor-singlet baryon is problematic because of its decay to $\Sigma(1385)\pi$, as $\mathbf{1} \nrightarrow \mathbf{10} + \mathbf{8}$ [21], so that invoking mixing with a higher resonance, presumably the 1690, belonging to a flavor octet according to other work [12] seems necessary.

Also, in the negative parity sector [19], an interesting quenched lattice calculation that separately analyzed the correlators found very similar octet and singlet masses for the $\Lambda\frac{1}{2}^-$ (and this around 1.6 GeV in agreement with [13]). That could indicate that in that channel, an octet and a singlet should appear almost degenerate and mixed, which seems to be the case for the $\Lambda(1380) - \Lambda(1405)$ system (though at a smaller mass consistent with a strong nucleon-meson open channel influence). However, the extent to which this system can be considered qqq remains questionable: This system might be mixed, but not be so relevant for our thrust.

There does not seem to be much information in the octet-singlet comparison for higher excitations or for the $\frac{3}{2}^+$ channel, but we can draw from the active field on Λ_c and Λ_b spectroscopy: For example, an excited likely $\Lambda_b\frac{1}{2}^+$ candidate has just been reported [23] (see, for example, [24] for quark-based theory discussion thereof).

In Fig. 1 we have displayed the Λ spectrum against the Λ_c, Λ_b (and marked the rescaled second shell of the ^{3}He atomic $A - e - e$ three-body system) as a benchmark.
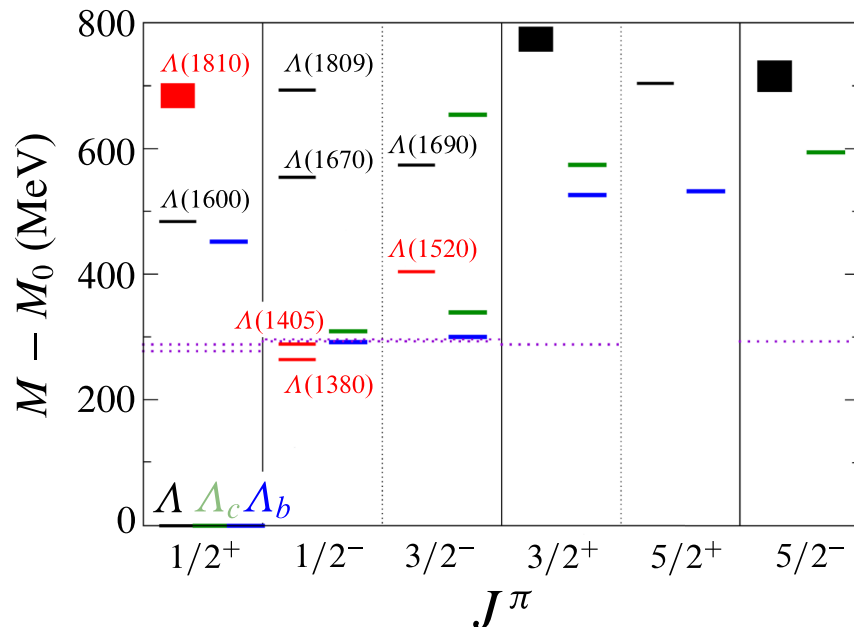
FIG. 1. Comparative of the Λ spectrum with the known Λ_c and Λ_b states that mark ideal *udc* and *udb* valence mixing without $SU(3)$ symmetry. To discuss the congruence of the spectra, we plot $M - M_0$ with $M_0 = 1116, 2286, 5620$ MeV, for s, c, b, respectively (and in the same spirit, the second shell levels of helium with $A = 3$ are also marked as dotted lines, with energies rescaled to match the $\Lambda_b\frac{1}{2}^-$). The Λ_S singlet candidates highlighted by the Graz group [12] (1810, 1405/1380, 1520) are displayed in red online.

The ground-state energy of all of them has been subtracted, so that only the excitation energy is seen in the plot.

As has been known for long, the charmed/charmonium and bottomed/bottomonium system have congruent spectra on this type of Grotrian diagram (see, e.g., [25]). This is due to the shape of the interquark Cornell linear + Coulomb potential that looks, in the momentum range where both pieces are of comparable magnitude, somewhat like a logarithmic potential (that would show actual matching of the spectra upon subtracting the ground state).

The heavy-baryon spectrum shown in the figure should correspond to the pure valence or ideally mixed configurations $(ud)c$, $(ud)b$ with little or no further flavor configuration mixing expected to affect the heavy quark, which is distinguishable and more localized than the others due to its large mass. The figure teaches us that the splittings to the ground state are generically larger for the strange Λ states than their heavy-quark counterparts, probably due to these being less relativistic, but they seem rather comparable. This suggests perhaps that one quantum of excitation costs a similar amount whether concentrated in a part of the system such as in $(ud)b$ or distributed through the three quarks such as in $(uds)_8$ or $(uds)_1$. Our findings within the Coulomb-gauge approach (see again Table I) would however indicate that the singlet qqq configuration can be a bit heavier in the Cornell linear + Coulomb potential.

Flavor mixing in the QCD Hamiltonian resides exclusively in the quark mass matrix, that for exact isospin symmetry can be written as

$$[M] = \frac{m_u + m_d + m_s}{3}\mathbb{I} - \frac{m_s - (m_u + m_d)/2}{\sqrt{3}}\lambda_8. \quad (3)$$

Since the second term, not respecting $SU(3)$ symmetry, is in the octet representation as Gell-Mann's λ_8 matrix reveals, singlet and octet hyperon representations can be mixed, but not singlet and decuplet ones. The Bonn group has extended [15] their earlier work to explore additional sources of flavor violation in an effective qqq Hamiltonian that is meant to incorporate effects of meson exchange among quarks in a potential. Because mesons have rather different masses, this potential is strongly flavor dependent.

In our own calculation in Sec. IV, we have kept the canonical interaction with the global symmetries of QCD, so that our flavor violation is reduced to the quark mass matrix in Eq. (3). Moreover, because dynamical chiral symmetry breaking means that the running quark mass decreases with the scale (unlike in constituent models where the mass is fixed; this point will be clear in Fig. 6 below), our approach should have significantly less flavor mixing than others. This probably oversimplifies a more complex physical picture, but makes discussion of the flavor-singlet configuration, whose absence in the low spectrum is the telltale of color, more straightforward.

To conclude this section, though it is often manifested that quark models cannot be used for precision work, which is fair criticism given the uncontrolled approximations that are needed to reduce them to manageable calculations, the prediction of the quantum numbers for the lowest Λ

excitations is spot on: Indeed, the first excitation in the quark model can have quantum numbers $J^\pi = \frac{1}{2}^-, \frac{3}{2}^-, \frac{1}{2}^+$ as demonstrated next in Sec. II. These happen to be the quantum numbers of the first few experimentally detected states, a refreshing agreement, so there are several possible candidates to the Λ_S singlet.

II. CONSTRUCTION OF VARIATIONAL WAVE FUNCTIONS FOR LOWEST-LYING qqq FLAVOR-SINGLET BARYONS

As discussed in Sec. I A, the $SU(3)$ flavor-singlet qqq baryon is in an antisymmetric flavor combination, and because of the confinement hypothesis, also antisymmetric in color, with Fermi statistics necessarily leaving an antisymmetric spin and spatial wave function of its valence quarks.

We employ configurations with well-defined total angular momentum $J := |\mathbf{J}|$, third component $\langle J_z \rangle$, and parity π. To obtain J, we combine the doublet representations from spin and spatial quantum numbers, which are a set of mixed-symmetric and mixed-antisymmetric configurations. The spatial part carries standard spherical harmonics $Y_l^m(\hat{k}_i)$ with $\hat{k}_i = \mathbf{k}_i / k_i$, $\mathbf{k}_i$ being the quark momentum and $k_i = |\mathbf{k}_i|$ its modulus.

With only one quark excited above the ground state, we can construct three different J^π combinations with totally antisymmetric spin-spatial states,
  (1) $1/2^+$ with a radial-like excitation $R_1(k)Y_0^0(\hat{k})$ [see Eq. (10) below]
  (2) $3/2^-$ with an angular excitation $R_0(k)Y_1^m(\hat{k})$ [see Eq. (11) below]
  (3) $1/2^-$, also with an angular excitation $R_0(k)Y_1^m(\hat{k})$ [see Eq. (12) below]
The two quarks that remain in the ground state are naturally assigned wave functions $R_0(k)Y_0^0(\hat{k})$. The three quarks are then antisymmetrized without concern about their mass/flavor (the flavor wave function is by construction antisymmetric itself). It is this step that suppresses any singlet-octet flavor mixing that may lower the mass: All results in this work refer to the pure flavor-singlet configuration. In a Λ_c or Λ_b baryon, one quark is in a definite flavor state; not here, all three have some probability amplitude of being the strange quark.

As explained in Sec. I A, we need to introduce that spatial excitation in order to build an antisymmetric spin-spatial wave function appropriate for the singlet baryon. Hence, we have two spin quantum states ($\pm 1/2$), and either two radial states ($n_r \in \{0, 1\}$ ground/excited) or two angular states ($l \in \{0, 1\}$). In each of these spaces, we therefore have a doublet of an $SU(2)$-like group, and for three quarks we have a tensor product, which furnishes a reducible representation thereof,

$$\mathbf{2} \otimes \mathbf{2} \otimes \mathbf{2} = \mathbf{4} \oplus \mathbf{2} \oplus \mathbf{2}. \tag{4}$$

The quadruplet **4** in the resulting direct-sum decomposition is totally symmetric under permutations of the three quarks, so joint antisymmetry of the spin-space wave function demands the usage of the two doublets **2**. These can be related to a couple of mixed-symmetric (MS) and mixed-antisymmetric (MA) states for spin $\chi_{MS,MA}(S, M_S)$

$$\chi_{MS}\left(\frac{1}{2}, \frac{1}{2}\right) = \frac{1}{\sqrt{6}} (2|\uparrow\uparrow\downarrow\rangle - |\uparrow\downarrow\uparrow\rangle - |\downarrow\uparrow\uparrow\rangle),$$

$$\chi_{MS}\left(\frac{1}{2}, -\frac{1}{2}\right) = \frac{1}{\sqrt{6}} (2|\downarrow\downarrow\uparrow\rangle - |\downarrow\uparrow\downarrow\rangle - |\uparrow\downarrow\downarrow\rangle),$$

$$\chi_{MA}\left(\frac{1}{2}, \frac{1}{2}\right) = \frac{1}{\sqrt{2}} (|\uparrow\downarrow\uparrow\rangle - |\downarrow\uparrow\uparrow\rangle),$$

$$\chi_{MA}\left(\frac{1}{2}, -\frac{1}{2}\right) = \frac{1}{\sqrt{2}} (|\downarrow\uparrow\downarrow\rangle - |\uparrow\downarrow\downarrow\rangle), \tag{5}$$

a construction that is immediately exported to orbital angular states $|L, M_L\rangle_{MS,MA}$,

$$|1, M_L\rangle_{MS} = \frac{1}{\sqrt{6}} (2|001_{M_L}\rangle - |01_{M_L}0\rangle - |1_{M_L}00\rangle),$$

$$|1, M_L\rangle_{MA} = \frac{1}{\sqrt{2}} (|01_{M_L}0\rangle - |1_{M_L}00\rangle), \tag{6}$$

and to orbital radial ones $|\mathrm{rad}\rangle_{MS,MA}$,

$$|\mathrm{rad}\rangle_{MS} = \frac{1}{\sqrt{6}} (2|001\rangle - |010\rangle - |100\rangle),$$

$$|\mathrm{rad}\rangle_{MA} = \frac{1}{\sqrt{2}} (|010\rangle - |100\rangle). \tag{7}$$

Combining these states, we can form antisymmetric combinations of the spin-orbital ones

$$|M_S; M_L\rangle = \frac{1}{\sqrt{2}} (\chi_{MS}(1/2, M_S)|1, M_L\rangle_{MA} - \chi_{MA}(1/2, M_S)|1, M_L\rangle_{MS}) \tag{8}$$

or of the spin-radial ones

$$|M_S; \mathrm{rad}\rangle = \frac{1}{\sqrt{2}} (\chi_{MS}(1/2, M_S)|\mathrm{rad}\rangle_{MA} - \chi_{MA}(1/2, M_S)|\mathrm{rad}\rangle_{MS}). \tag{9}$$

Once fully antisymmetric representations of the quark permutation group are achieved, the Clebsch-Gordan coefficients assist in obtaining antisymmetric spin-spatial wave functions with well-defined J^π. As advanced, with only one quantum excitation there are three cases, in agreement with earlier work [12]

$$|1/2^+\rangle = |M_S = 1/2; \mathrm{rad}\rangle, \tag{10}$$

$$|3/2^-\rangle = |M_S = 1/2; M_L = 1\rangle, \qquad (11)$$

$$|1/2^-\rangle = \sqrt{\frac{2}{3}}|M_S = -1/2; M_L = 1\rangle$$
$$+ \frac{1}{\sqrt{3}}|M_S = 1/2; M_L = 0\rangle. \qquad (12)$$

This resulting collection of quantum numbers is used to prepare the necessary effective Lagrangians to study branching fractions of flavor-singlet baryon decay at the hadron level in Sec. III below.

Additionally, these wave functions are also injected into the Rayleigh-Ritz variational principle $\langle \psi_S | H | \psi_S \rangle \le E_S \langle \psi_S | \psi_S \rangle$ with the quark-level Hamiltonian specified below in Sec. IV.

Symmetry considerations do not fix the wave functions entirely, leaving what are usually called "radial" excitations in Eq. (7) (a concept that makes sense once the three-body variables have been fixed).

We have employed three different variational radial *Ansätze* in closed analytical form. Each is a family of functions with up to three variational parameters ρ_i, one for each quark. Because we impose the center-of-mass $\sum \mathbf{k}_i = \mathbf{0}$ condition, one of the parameters is redundant; we prefer to dedicate the additional computer time spent in the redundancy than further complicating the wave functions. They read

$$R_n^{(0)}(k) = \begin{cases} \left[\left(\frac{k}{\rho}\right)^2 + 1 \right]^{-2} & \text{for } n = 0, \\ \frac{2}{[(\frac{k}{\rho})^2 + 1]^2} + \frac{(\frac{k}{\rho})^2 - \frac{3}{4}}{[(\frac{k}{\rho})^2 + \frac{1}{4}]^3} & \text{for } n = 1, \end{cases} \qquad (13)$$

$$R_n^{(1)}(k) = \begin{cases} \frac{k}{\rho} e^{-(\frac{k}{\sqrt{2}\rho})^2} & \text{for } n = 0, \\ \left[2\left(\frac{k}{\rho}\right)^3 - 3\frac{k}{\rho} \right] e^{-(\frac{k}{\sqrt{2}\rho})^2} & \text{for } n = 1, \end{cases} \qquad (14)$$

$$R_n^{(2)}(k) = \begin{cases} \left[\frac{3}{2} - \left(\frac{k}{\rho}\right)^2 \right] e^{-(\frac{k}{\sqrt{2}\rho})^2} & \text{for } n = 0, \\ \left[\frac{15}{4} - 5\left(\frac{k}{\rho}\right)^2 + \left(\frac{k}{\rho}\right)^4 \right] e^{-(\frac{k}{\sqrt{2}\rho})^2} & \text{for } n = 1. \end{cases} \qquad (15)$$

The first one corresponds to a hydrogenlike wave function, the second to a one-dimensional harmonic oscillator, and the third one is related to the three-dimensional harmonic oscillator. These wave functions can be employed to apply the variational principle to any appropriate QCD or QCD-like Hamiltonian.

Finally, we employ a fourth wave function family which is implemented as a numeric table to be interpolated. The table is obtained by solving the 1^{--} meson problem with the same Hamiltonian and potential parameters later used for the three-body problem

$$R_n^{(3)}(k) = \begin{cases} \psi_\rho(k) & \text{for } n = 0, \\ \psi_{\rho'}(k) & \text{for } n = 1, \end{cases} \qquad (16)$$

where the ρ two-body problem was simplified by ignoring d-wave or backpropagating Salpeter (random phase approximation) contributions, so that the two wave functions with $n = 0, 1$ are adequately orthogonal in the radial k variable (without being concerned about the precision reached in the ρ spectrum, that does require the additional contributions).

The hope is that this wave function, by having the correct tails for the interaction, will be able to relax $\langle H \rangle$ somewhat more than the others (this will be shown to be the case in one instance, the $\frac{1}{2}^+ \Lambda_S$, whereas for the other quantum number combinations, $R_n^{(0)}$ performs equally well, so we will quote results therefrom as it is more straightforward).

But before deploying a specific calculation, we dedicate Sec. III to exploiting our gained knowledge of the possible quantum numbers in the low spectrum to discuss Λ_S decays.

III. DECAY BRANCHING RATIOS OF THE $SU(3)$-FLAVOR SINGLET BARYON AS FUNCTION OF ITS MASS

In this section, we will employ the simplest methods of effective theory (EFT) to learn about the relevant two-body (Secs. III A and III B) and, only for one case, three-body (Sec. III C) decay widths of the Λ_S baryon, without attempting to probe its internal structure, but exploiting flavor symmetry and phase space to relate different decay channels. The overall decay constant of the effective Lagrangians below, such as Eqs. (18), (22), and (27), will be left undetermined, so that predictivity extends only to branching fractions $\Gamma_i / \Gamma_{\text{total}}$.

This is of interest, from a purely experimental point of view, to eventually understand how well the existing physical baryons with the same quantum numbers match a pure singlet configuration, but also to explore the influence of the open channels to the seed qqq baryons that quark approaches produce. Naturality suggests that the imaginary part of the baryon propagator (thus, the decay width) is of similar size to the correction to the real part, shifting its mass (that, at order zero, is seeded by the pure quark calculations discussed below in Sec. V). This section employs standard notation of hadron effective theory: B will represent the ground-state baryon flavor octet of Gell-Mann, and Φ the pseudoscalar meson octet.

A. Two-body decays with a contact Yukawa Lagrangian

We consider first two-body $B\phi$ baryon-meson decays of the singlet Λ_S, that is, $\Lambda_S \to B + \phi$ decay.

In this subsection, we adopt the simplest contact Yukawa Lagrangian density. This is analogous to the analysis of

flavor in baryon decays carried out by Guzey and Polyakov [21] (though they cover the entire spectrum) to which we refer for extensive discussion. They find the ratios among coupling constants, exclusively based on the flavor structure, given by $g_{\Lambda_S NK} : g_{\Lambda_S \Sigma\pi} : g_{\Lambda_S \Lambda\eta} : g_{\Lambda_S \Xi K} = \frac{1}{2} : \sqrt{\frac{3}{2}} : -\frac{1}{2\sqrt{2}} : -\frac{1}{2}$ and whose squares give a first idea of the relative importance of the different two-body decay channels.

Such coefficients are hidden from direct experimental access due to two problems that are adding up for states of low and moderate mass. The first is the phase-space integral: If states are not too far from the respective thresholds (or even below, with zero width), the $SU(3)$ relations of the couplings are completely wiped out by the large $SU(3)$ breaking induced by the very different momenta, in turn coming from the decay-product masses by Källen's formula $|\boldsymbol{p}| = \frac{1}{2m_{\Lambda_S}} \lambda^{1/2}(m_{\Lambda_S}^2, m_1^2, m_2^2)$. This first issue is easily addressed by proceeding to the total width that can be given in numeric form to compare with experiment,

$$\Gamma(\Lambda_S \to 1 + 2) = \frac{|\boldsymbol{p}|}{32\pi^2 m_{\Lambda_S}^2} \int |\mathcal{M}|^2 d\Omega. \quad (17)$$

To get rid of the model dependence of the g_i, we plot $\frac{\Gamma_i}{\sum_{2\,\mathrm{body}} \Gamma_i}$ in Fig. 2 (top plot). The detailed discussion of such plots is postponed to Sec. III B, but let us note here how all channels tend to a constant (energy-independent) decay fraction at large decaying-particle mass (flavor symmetry) whereas, at low momenta, different phase space makes the various lines immensely different.

The second problem with a constant coupling is that the pion and, to a lesser extent, the kaon and the eta are quasi-Goldstone bosons, and the construction of chirally symmetric Lagrangians demands that they are derivatively coupled. Constant, momentum-independent couplings, can of course be present too, since chiral symmetry is not exact, but the large derivatively coupled contribution can enhance the apparent $SU(3)$-symmetry breaking of the decay by the same mechanism, the different momenta induced by the different masses.

B. Two-body decays with a derivatively coupled meson

After the brief example of a constant Yukawa coupling, we proceed to examine the derivatively coupled meson Lagrangian for all three J^π combinations of interest for a qqq Λ_S.

1. State with $J^\pi = \frac{1}{2}^+$

We use the simplest perturbative Lagrangian with a pion derivative coupling as suggested by the chiral theory of the strong interactions [26] and $SU(3)$ symmetry,

$$L = -\frac{g}{2f_\pi} \bar{\Psi}_{\Lambda_S} \gamma_\mu \gamma_5 \mathrm{tr}(\Psi_B \partial^\mu \Phi), \quad (18)$$
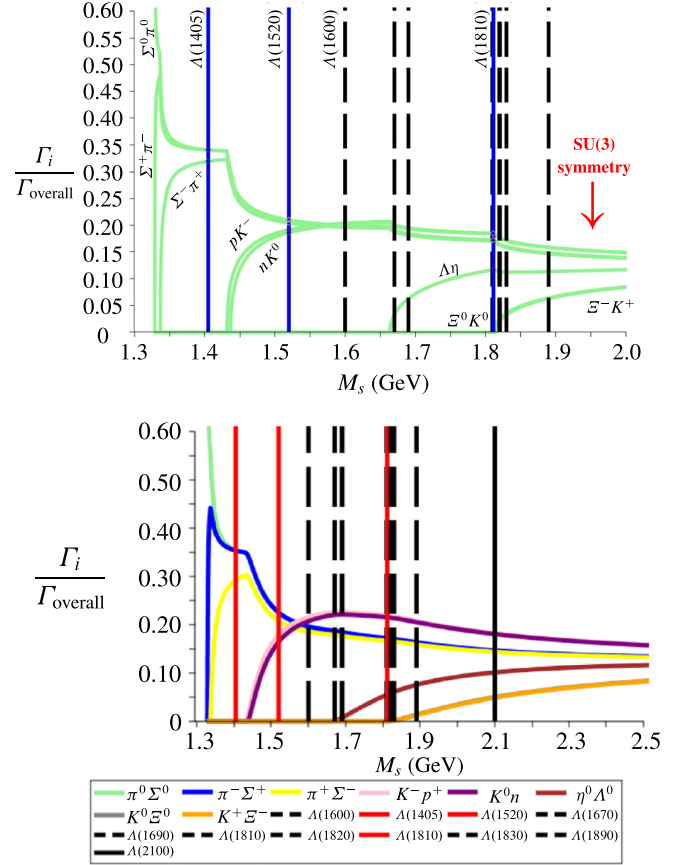

FIG. 2. Branching ratios of the two-body flavor-preserving decay channels of the $SU(3)$ singlet Λ_S as function of $M_s := m_{\Lambda_S}$ for $J^\pi = \frac{1}{2}^+$. The top plot shows the case of a constant Yukawa vertex, whereas the bottom plot employs the derivatively coupled amplitude of Eq. (20).

where g is the decay coupling and f_π the weak meson decay constants, both flavor independent, Ψ_B is the octet and Ψ_{Λ_S} the singlet baryon fields, and Φ is the meson field (the flavor trace is taken over the product of the two octet matrices). It yields a matrix element

$$|\mathcal{M}|^2$$
$$= \mathrm{Tr}((\not{p}_{\Lambda_S} - \not{p}_B)\gamma_5(\not{p}_{\Lambda_S} + m_{\Lambda_S})\gamma_5(\not{p}_B - \not{p}_{\Lambda_S})(\not{p}_B + m_B)) \quad (19)$$

that is especially simple if evaluated in the rest frame of the decaying Λ_S baryon,

$$\overline{|\mathcal{M}|^2} = (m_{\Lambda_S} + m_B)^2((m_{\Lambda_S} - m_B)^2 - m_\phi^2) \quad (20)$$

in terms of the respective masses.

The two-body flavor-preserving decay channels of the $SU(3)$ singlet Λ_S are $\Sigma^0\pi^0$, $\Sigma^+\pi^-$, $\Sigma^-\pi^+$, pK^-, nK^0, $\Lambda^0\eta/\eta'$, $\Xi^0 K^0$, and $\Xi^- K^+$. Their branching ratios are presented in the lower plot of Fig. 2 (bottom plot).

The vertical solid lines (red online) correspond to the three Λ resonances in the 1.4–2 GeV region that are candidates to be (or to contain a sizeable amount of the wave function of) the lightest flavor singlet as per the Graz proposed assignment [12]. The rest of the lines represent various other Λ_S resonances. If we take the current J^π assignments of the Particle Data Group at face value, $\Lambda(1600)$ and $\Lambda(1810)$ are the lightest relevant ones (Sec. I B)

To exemplify the use of such graphs, let us focus on the $\Lambda(1600)$ that the Graz group classified as belonging to a first excited octet with $\frac{1}{2}^+$ including the $N(1440)$ Roper resonance. It corresponds to the first vertical dashed line. From the graph, we see that there are five channels with an approximately equal branching fraction if the state is a singlet instead, the three $\pi\Sigma$ charge combinations and the two KN ones. This entails a prediction $\Gamma_{\pi\Sigma}/\Gamma_{KN} \simeq 1.5$ that would be informative in possession of more accurate experimental data (currently, the PDG average is consistent with a broad interval $\Gamma_{\pi\Sigma}/\Gamma_{KN} \simeq 1.1$–3.1).

2. State with $J^\pi = \frac{1}{2}^-$

If the Λ_S state has parity opposite to the nucleon, the decay vertex equivalent to Eq. (18) will lack the γ_5 so that the total Lagrangian density is parity even, as corresponds to the strong force. In that case, Eq. (20) turns into

$$\overline{|\mathcal{M}|^2} = (m_{\Lambda_S} - m_B)^2((m_{\Lambda_S} + m_B)^2 - m_\phi^2). \quad (21)$$

The resulting relative two-body decay intensities are shown in Fig. 3.

For example, a singlet state with the mass of $\Lambda(1670)$ would decay in the ratios $KN:\pi\Sigma:\eta\Lambda = 1:0.7:0.1$ approximately, whereas the experimental quotients seem to be $1:0.3$–$0.7:0.4$–1.4. Thus, current experimental data are not yet at the precision level where they could exclude this particle from a singlet assignment just from its decays (one needs to resort to Gell-Mann-Okubo-type arguments seeing whether the state fits well inside a complete baryon octet or not).

3. State with $J^\pi = \frac{3}{2}^-$

The third basic excitation that can form a qqq flavor singlet has spin-$\frac{3}{2}$. This requires the use of a higher representation of the Lorentz group than conventional spinors: A convenient formalism is that of Rarita and Schwinger. While it is usually not covered in basic treatments, it is somewhat widely known, so we compromise by giving the detail of the calculation but relegating it to Appendix A. The decay vertex is now

$$L = g_{\Lambda_S B\phi} \mathrm{tr}[\bar{\Psi}_B (P^{3/2})^{\mu\nu}(\Psi_{\Lambda_S RS})_\nu \partial_\mu \Phi] + \text{H.c.}, \quad (22)$$

where $(\Psi_{\Lambda_S RS})_\nu$ is the Rarita-Schwinger collection of spinors described in Appendix A and $(P^{3/2})^{\mu\nu}$ the projector
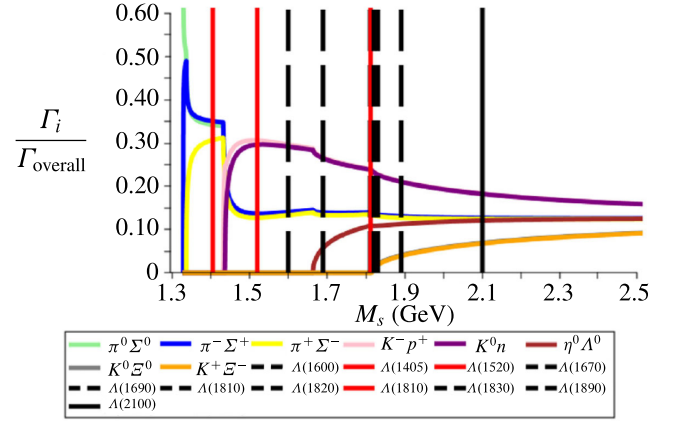

FIG. 3. Branching ratios of the two-body flavor-preserving decay channels of the $SU(3)$ singlet Λ_S as function of $M_s := m_{\Lambda_S}$ for $J^\pi = \frac{1}{2}^-$.

necessary to pick up the spin-$\frac{3}{2}$ component therefrom. The flavor trace has also been taken so the Lagrangian density is a flavor singlet. This leads to a squared matrix element

$$\overline{|\mathcal{M}|^2} = (p_{\Lambda_S} - p_B)_\mu (-p_{\Lambda_S} + p_B)_\nu \\ \times \mathrm{Tr}((P^{3/2})^{\mu\nu}(\not{p}_{\Lambda_S} + m_{\Lambda_S})(\not{p}_B + M_B)). \quad (23)$$

Since the projector $P^{3/2}$ somewhat complicates the calculation, we have carried it out with the help of the symbolic manipulation system FORM [27]. We organize the result as a power-series expansion in m_{Λ_S}, yielding

$$\overline{|\mathcal{M}|^2} \propto \frac{1}{3} m_{\Lambda_S}^4 + \frac{2}{3} m_{\Lambda_S}^3 m_B - m_{\Lambda_S}^2 \left(m_\phi^2 + \frac{1}{3} m_B^2 \right) \\ - \frac{4}{3} m_{\Lambda_S} (m_\phi^2 + m_B^2) m_B - \left(\frac{1}{3} m_B^4 + \frac{2}{3} m_B^2 m_\phi^2 - m_\phi^4 \right) \\ + \frac{2}{3} \frac{m_B}{m_{\Lambda_S}} (m_B^2 - m_\phi^2)^2 \\ - \frac{1}{m_{\Lambda_S}^2} \left(\frac{1}{3} m_\phi^6 - m_B^2 m_\phi^4 + m_B^4 m_\phi^2 - \frac{1}{3} m_B^6 \right). \quad (24)$$

After folding it with phase space, the resulting relative two-body branching fractions are plotted in Fig. 4, with conventions equal to those of Fig. 2.

We find it remarkable that the KN channel is always substantially below the $\pi\Sigma$ one. This prediction of the lowest derivatively coupled Lagrangian for the decay of a spin-$\frac{3}{2}$ particle basically discards all experimental candidates to be $\Lambda_S \frac{3}{2}^-$. For example, for the $\Lambda(1520)$, the measurement for the ratio $\Gamma_{\pi\Sigma}/\Gamma_{KN} \sim 1$, whereas the prediction is a factor 9 (this is driven by the small phase space available for KN, but also on dynamical grounds). While less extreme, the problem remains for the $\Lambda_S(1690)$
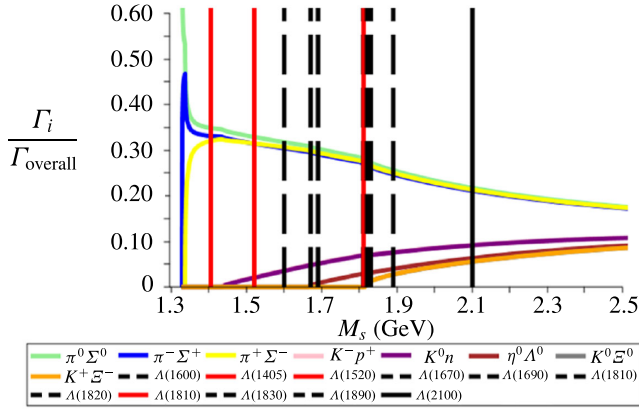
FIG. 4. Branching ratios of the two-body flavor-preserving decay channels of the $SU(3)$ singlet Λ_S as function of $M_s := m_{\Lambda_S}$ for $J^\pi = \frac{3}{2}^-$.

and higher reported candidates (less solid) with these quantum numbers.

C. Decay into three particles

Though data on three-body decays of excited hyperons are scant, it may be of interest to think about them, at least for the one singlet candidate with the largest phase space, the heavier $\frac{1}{2}^+$. For these $\Lambda_S \to B + \phi + \phi$ decay processes, it is of note that two different $SU(3)$-singlet combinations can be formed in the final state with an octet baryon and two octet mesons as

$$\mathbf{8} \otimes \mathbf{8} \otimes \mathbf{8} = \mathbf{1} \oplus \mathbf{1} \oplus \cdots, \tag{25}$$

so that full specification of the final state requires a mixing angle

$$|\psi_2 \phi_3 \phi_4\rangle = \cos\theta_M |S_1\rangle + \sin\theta_M |S_2\rangle, \tag{26}$$

which we have adopted for this example, as $\theta_M = \frac{\pi}{4}$ (maximal mixing of the two singlets).

The construction of an appropriate chiral Lagrangian demands one of the mesons to be derivatively coupled, so that an appropriate effective vertex for a $\frac{1}{2}^+$ hyperon would be [26]

$$L = \frac{i}{8f_\pi^2} [\text{tr}(\bar{\Psi}_B \Phi \partial^\mu \Phi) + \text{tr}(\Phi \bar{\Psi}_B \partial^\mu \Phi)] \gamma_\mu \Psi_{\Lambda_S}, \tag{27}$$

where f_π is the weak pion decay constant, Ψ_{Λ_S} is the singlet baryon field, Ψ_B the ground-state octet baryon, and Φ the octet meson fields, respectively. The trace over the flavor index is sensitive to the ordering of the fields.

The tree-level matrix element, up to species-independent constants, follows from Eq. (27) to be

$$-i\mathcal{M} \equiv \langle \psi_2 \phi_3 \phi_4 | \mathcal{L}_{\text{eff}} | \Lambda_S \rangle$$
$$= (\langle S_1 | \cos\theta_M + \langle S_2 | \sin\theta_M) \mathcal{L}_{\text{eff}} | \Lambda_S \rangle$$
$$= \frac{1}{\sqrt{2}} \bar{u}(2) \gamma_\mu (p_3^\mu + p_4^\mu) u(1)/\sqrt{2}, \tag{28}$$

from which

$$\overline{|\mathcal{M}|^2} = (2m_1^2 + m_3^2 + m_4^2 - m_{23}^2 - m_{24}^2)(m_1^2 - m_4^2 - m_{23}^2)$$
$$- m_3(m_{23}^2 + m_{24}^2 - m_3^2 - m_4^2) + 2m_1 m_2 m_3^2, \tag{29}$$

where m_1 is the mass of Λ_S in the center-of-momentum (cm) frame, m_2 is the mass of the baryon, m_3 and m_4 are the mass of the mesons, and m_{23} and m_{24} are the Dalitz variables

$$m_{23}^2 \equiv p_{23}^2 = (p_2 + p_3)^2, \quad m_{24}^2 \equiv p_{24}^2 = (p_2 + p_4)^2. \tag{30}$$

A few more details on these variables, particularly to define the physical region over which the squared matrix element of Eq. (29) is integrated, are left for Appendix B.

A flavor-symmetry-preserving decay of a flavor-singlet hyperon can yield the particle combinations listed in Table II.

The total width, and now also the branching ratios of these channels, are not rigorously accessible because the coupling constants in Eqs. (27) and (18) are not related in a model-independent way known to us, so that we cannot predict the ratio of three- to two-body decay fractions. What can be done is to once more exploit the symmetry structure built into Eq. (27) to predict the relative strength of three-body channels with respect to each other. This relative strength $\Gamma_i / \Gamma(3\,\text{body})$ is plotted in Fig. 5.

To exemplify, let us for a moment take the $\Lambda(1810)$ as the lightest $\Lambda_S \frac{1}{2}^+$ candidate at face value, though a new data analysis suggests that it might be a surplus resonance not really necessary to obtain an optimal global data fit [22]. No three-body decays seem to have been experimentally reported.

At the position of this $\Lambda(1810)$ (vertical line in Fig. 5), we see that $\Lambda\pi\pi$, the channel with the lowest threshold, starts losing its phase-space advantage, so that it is still dominant but comparable to $NK\pi$ (that becomes dominant for even higher masses) due to the derivative coupling of Eq. (27), and about a factor of 2 larger than $\Sigma\pi\pi$, with other decay channels being kinematically closed at that energy.

TABLE II. Three-body channels available for $SU(3)$-symmetry-preserving decay of Λ_S. Their relative branching fractions with $J^\pi = \frac{1}{2}^+$ are given in Fig. 5.

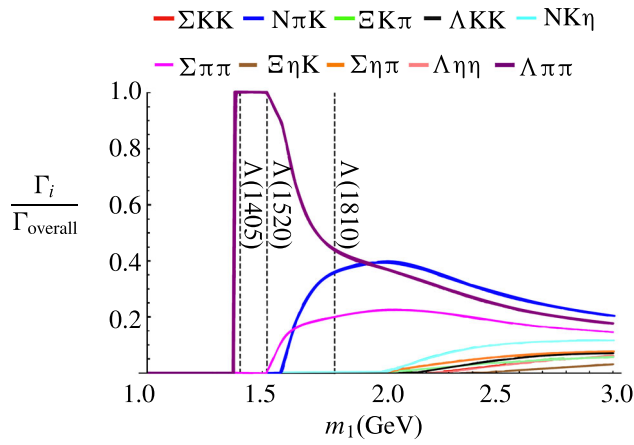| Baryon	Σ	N	Ξ	Λ	N	Σ	Ξ	Σ	Λ	Λ
First meson	K	π	K	K	K	π	η	η	η	π
Second meson	K	K	π	K	η	π	K	π	η	π

FIG. 5. Relative strength of the three-body decays in the limit of exact $SU(3)$ symmetry.

IV. ESTIMATE OF SINGLET MASS IN THE NCSTATE COULOMB-GAUGE QCD MODEL: THEORETICAL FRAMEWORK

To attempt a numerical estimation of the actual qqq singlet masses (as past work mostly took uds configurations without a flavor separation), we employ a well-known Hamiltonian model obtained from Coulomb-gauge QCD. Its philosophy dating back to [28–30] is to use a field-theory formalism maintaining the global symmetries of QCD so that chiral symmetry breaking is spontaneous and not explicit as in the nonrelativistic quark model. The interaction corresponds to the established Cornell potential for heavy quarkonium with the appropriate color factors, and the flavor structure of the spectrum is reasonable; it can be seen as an extension of the Cornell model [31] to include gluodynamics.

This approach gave a reasonable explanation of the lattice glueball spectrum [32,33], basic features of quark-antiquark mesons, and of three-quark baryons, and was deployed early on to show that 1^{-+} exotic mesons cannot be very light [34,35] (unlike mainstream thought at the time), to study internal $b\bar{b}$ structure [36] abstracting model-independent features, and to study the coupling [37] of $q\bar{q}$ and $qq\bar{q}\bar{q}$ configurations [38], with hints that this mixing would provide an explanation for ideal $\omega - \phi$ vector meson mixing.

The most recent works within the model's approach have been carried out by Abreu *et al.* [39–41] in studying conventional $q\bar{q}$ spectroscopy in less trodden channels. Thus, the model is a one-stop Hamiltonian for many issues in spectroscopy. On the downside, because it is an equal-time quantization approach, it is not useful to compute form factors or other functions pertaining to hadron structure, for which the Dyson-Schwinger+Bethe-Salpeter/Faddeev [42], or the light-front [43] or point form [44] approaches are more apt.

The quark part of the Hamiltonian is described in [45] and contains a kinetic term $H_{\rm kin}$, the longitudinal

Coulomb-potential interaction V_C that accommodates asymptotic freedom at small distances and confinement at large distances, and an effective transverse interaction V_T that represents the hyperfine quark-gluon interaction. It can be written in second quantization as

$$H = H_{\rm kin} + V_C + V_T, \tag{31}$$

$$H_{\rm kin} = \int d^3\vec{x}\,\Psi^\dagger(\vec{x})(-i\vec{\alpha}\cdot\vec{\nabla} + m_f\cdot\beta)\Psi(\vec{x}), \tag{32}$$

$$V_C = -\frac{1}{2}\int d^3\vec{x}\,d^3\vec{y}\,\rho^a(\vec{x})V(|\vec{x}-\vec{y}|)\rho^a(\vec{y}), \tag{33}$$

$$V_T = \frac{1}{2}\int d^3\vec{x}\,d^3\vec{y}\,J_i^a(\vec{x})\left(\delta_{ij} - \frac{\nabla_i\nabla_j}{\nabla^2}\right)U(|\vec{x}-\vec{y}|)J_j^a(\vec{y}). \tag{34}$$

Therein, the quark fields Ψ are used to construct a local color density ρ^a and current $\vec{J}^a(\vec{x})$ with the color Gell-Mann matrices T^a,

$$\rho^a(\vec{x}) = \Psi^\dagger(\vec{x})T^a\Psi(\vec{x}), \quad \vec{J}^a(\vec{x}) = \Psi^\dagger(\vec{x})\vec{\alpha}T^a\Psi(\vec{x}). \tag{35}$$

The kernel V has been presented in [30] as

$$V(q) = \begin{cases} C(q) = -\dfrac{8.07}{q^2}\dfrac{\log^{-0.62}(\frac{q^2}{m_g^2}+0.82)}{\log^{0.8}(\frac{q^2}{m_g^2}+1.41)} & \text{for } q > m_g, \\[4mm] L(q) = -\dfrac{12.25 m_g^{1.93}}{q^{3.93}} & \text{for } q < m_g, \end{cases} \tag{36}$$

where q is the modulus of the exchanged momentum. The model depends on a free parameter, the dynamical mass of the exchanged gluon, that takes a value [45] $m_g = 0.6$ GeV, yielding an asymptotic string tensionlike scale of $\sqrt{8\pi\sigma}\,12.25^{1/1.93}m_g\simeq0.44$ GeV, that is, $\sigma \simeq 0.2$ GeV^2 sufficient for a reasonable description of the quarkonium spectrum.

The kernel U is introduced as *model 4* in [45]. It is a Yukawa-type potential of the form

$$U(q) = \begin{cases} C(q) & \text{for } q > m_g, \\[2mm] -\dfrac{C_h}{q^2+m_g^2} & \text{for } q < m_g. \end{cases} \tag{37}$$

[The constant $C_h \simeq (2.907 \text{ GeV})^3$ for $m_g = 0.6$ GeV simply guarantees continuity of $U(q)$ at the matching point.]

It is a natural implementation of the Coulomb-gauge philosophy that separates an infrared strong scalar potential and an infrared suppressed transverse one due to physical gluon exchange being affected by the dynamical mass m_g.

The quark field can be expanded in particle/antiparticle normal modes in momentum space,
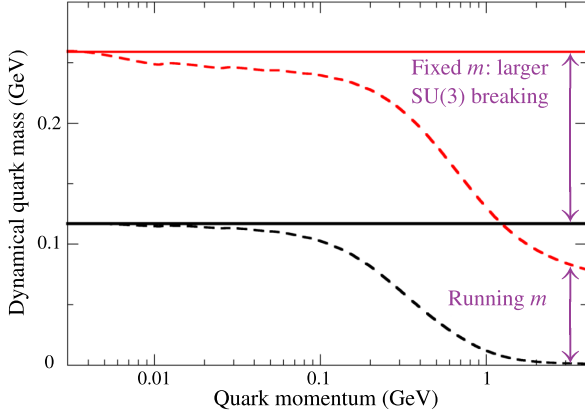
FIG. 6. Typical running quark mass $m(k)$ in the one-particle spinors solving the Hamiltonian model gap equation for the light and strange sector. The $SU(3)$-breaking scale $m_s - m_u \simeq$ 70 MeV at a high quark momentum is enhanced by dynamical chiral symmetry breaking and becomes a factor 2 larger at low momentum in this particular calculation. The constituent quark model, with a fixed quark mass instead, breaks $SU(3)$ with the same (larger) intensity at all scales.

$$\Psi(\vec{x}) = \int \frac{d^3\vec{k}}{(2\pi)^3} e^{i\vec{k}\vec{x}} \sum_{\lambda c f} (\mathcal{U}_{\vec{k}\lambda f} B_{\vec{k}\lambda f c} + \mathcal{V}_{-\vec{k}\lambda f} D^\dagger_{-\vec{k}\lambda f c}) \hat{e}_c \hat{\eta}_f.$$

(38)

λ, f, and c are indices for spin projection, flavor, and color, respectively, and $\hat{e}_c$, $\hat{\eta}_f$ are the color and flavor unitary vectors. The spinors $\mathcal{U}$, $\mathcal{V}$ are, in terms of the Pauli spinors (χ_λ), given by

$$\mathcal{U}_{\vec{k}\lambda f} = \frac{1}{\sqrt{2}} \left[\begin{array}{c} \sqrt{1 + s_{kf}} \chi_\lambda \\ \sqrt{1 - s_{kf}} \vec{\sigma} \cdot \hat{k} \chi_\lambda \end{array} \right],$$

(39)

$$\mathcal{V}_{-\vec{k}\lambda f} = \frac{1}{\sqrt{2}} \left[\begin{array}{c} -\sqrt{1 - s_{kf}} \vec{\sigma} \cdot \hat{k} i\sigma_2 \chi_\lambda \\ \sqrt{1 + s_{kf}} i\sigma_2 \chi_\lambda \end{array} \right],$$

(40)

where we have made use of the Bogoliubov angle ϕ_{kf} related to a running quark mass $m(k, f)$ and energy $E(k, f) = \sqrt{m^2(k, f) + k^2}$ in the following way:

$$s_{kf} = \sin\phi_{kf} = \frac{m(k, f)}{E(k, f)}, \quad c_{kf} = \cos\phi_{kf} = \frac{k}{E(k, f)}. \quad (41)$$

The gap equation that provides the model vacuum and one-particle dispersion relation was reported in an earlier work [45]. In Fig. 6, we plot a couple of typical $m(k)$ mass functions for quark momentum up to a few GeV. The generated quark mass seems somewhat smaller than usual in the constituent picture, but this is not remarkable in an approach where there is a significant self-energy in the potential part of the Hamiltonian [see Eq. (43) below].

It is clear that $SU(3)$ symmetry breaking by the effective quark mass is largest for zero momentum quarks and drops with the scale (just as it should in exact QCD). This leads us to expect less $SU(3)$ symmetry breaking (and therefore, less Λ_S-Λ_O singlet-octet mixing) than in constituent quark models: Those feature a constant quark mass which is scale independent, and therefore, the high-momentum wave function components support larger flavor-symmetry breaking.

Now with all these pieces and shortening $B_i = B_{\vec{k}_i, \lambda_i, f_i, c_i}$ for the ith quark, we can write down the state of our singlet baryon $|\Lambda_S\rangle$ with well-defined J^π in terms of a suitable combination of products of the spin-spatial *Ansätze* of each quark $F^{\lambda_1 \lambda_2 \lambda_3}_{\Lambda_S}(\{\vec{k}_i\})$ as

$$|\Lambda_S\rangle = \int \frac{d^3\vec{k}_1 d^3\vec{k}_2 d^3\vec{k}_3}{(2\pi)^9} \frac{\epsilon^{c_1 c_2 c_3}}{\sqrt{6}} \frac{\epsilon^{f_1 f_2 f_3}}{\sqrt{6}} \delta(\vec{k}_1 + \vec{k}_2 + \vec{k}_3)$$
$$\times F^{\lambda_1 \lambda_2 \lambda_3}_{\Lambda_S}(\{\vec{k}_i\}) B_1^\dagger B_2^\dagger B_3^\dagger |\Omega\rangle. \quad (42)$$

[In Eq. (42), summations over spin projection, flavor, and color are implicit.]

Hence, we can express the variational approximation to the Λ_S mass as

$$M_{\Lambda_S} = \langle \Lambda_S | H | \Lambda_S \rangle = 3 \int \frac{d^3\vec{k}_A d^3\vec{k}_B}{(2\pi)^6} [\mathcal{F}^{\lambda_A \lambda_B \lambda_C}_{\Lambda_S}(\vec{k}_A, \vec{k}_B)]^\dagger \left\{ \sum_{f_A} \frac{c_{k_A f_A} |\vec{k}_A| + m_{f_A} s_{k_A f_A}}{3} \mathcal{F}^{\lambda_A \lambda_B \lambda_C}_{\Lambda_S}(\vec{k}_A, \vec{k}_B) - \frac{2}{3} \frac{d^3\vec{q}}{(2\pi)^3} \right.$$

$$\times \left(V(|\vec{q}|) \left[\mathcal{F}^{\lambda_A \lambda_B \lambda_C}_{\Lambda_S}(\vec{k}_A, \vec{k}_B) \sum_{f_A} \frac{1}{3} (s_{k_A f_A} s_{k_A + q, f_A} + c_{k_A f_A} c_{k_A + q, f_A} \cdot x) - \frac{1}{6} \sum_{\substack{f_A f_B \\ f_A \neq f_B}} \mathcal{U}^\dagger_{\vec{k}_A \lambda_A f_A} \mathcal{U}_{\vec{k}_A + \vec{q}, \lambda_a f_A} \mathcal{U}^\dagger_{\vec{k}_B \lambda_B f_B} \mathcal{U}_{\vec{k}_B - \vec{q}, \lambda_b f_B} \right. \right.$$

$$\times \mathcal{F}^{\lambda_a \lambda_b \lambda_C}_{\Lambda_S}(\vec{k}_A + \vec{q}, \vec{k}_B - \vec{q}) \right] + U(|\vec{q}|) \left[\sum_{f_A} \frac{1}{3} \left(2 s_{k_A f_A} s_{k_A + q, f_A} + 2 c_{k_A f_A} c_{k_A + q, f_A} \frac{x(k_A^2 + (\vec{k}_A + \vec{q})^2) - |\vec{k}_A + \vec{q}| k_A (1 + x^2)}{q^2} \right) \right.$$

$$\left. \left. \left. \times \mathcal{F}^{\lambda_A \lambda_B \lambda_C}_{\Lambda_S}(\vec{k}_A, \vec{k}_B) - \sum_{\substack{f_A f_B \\ f_A \neq f_B}} \mathcal{U}^\dagger_{\vec{k}_A \lambda_A f_A} \alpha_i \mathcal{U}_{\vec{k}_A + \vec{q}, \lambda_a f_A} \frac{(\delta_{ij} - \hat{q}_i \hat{q}_j)}{6} \mathcal{U}^\dagger_{\vec{k}_B \lambda_B f_B} \alpha_j \mathcal{U}_{\vec{k}_B - \vec{q}, \lambda_b f_B} \mathcal{F}^{\lambda_a \lambda_b \lambda_C}_{\Lambda_S}(\vec{k}_A + \vec{q}, \vec{k}_B - \vec{q}) \right] \right) \right\}, \quad (43)$$

where we have employed the usual shorthand $x = \frac{\vec{k}_A}{|\vec{k}_A|} \cdot \frac{\vec{k}_A + \vec{q}}{|\vec{k}_A + \vec{q}|}$. Also, notice the difference among F_{Λ_S} in Eq. (42) and $\mathcal{F}_{\Lambda_S}$ in Eq. (43): The first is the product of the spatial *Ansätze* of the three quarks, while the last is its antisymmetrized form

$$\mathcal{F}_{\Lambda_S}^{\lambda_1 \lambda_2 \lambda_3} = \sum_{a,b,c} \epsilon^{abc} F_{\Lambda_S}^{\lambda_a \lambda_b \lambda_c}(\vec{k}_a, \vec{k}_b, \vec{k}_c), \{a, b, c\} \in \{1, 2, 3\}.$$

(44)

This fermion antisymmetry naturally appears due to the anticommutation rules of the creation and annihilation operators $B_i^\dagger, B_i$.

It remains to specify the parameters of the Hamiltonian. They are consistent with extensive meson work in the Coulomb-gauge model, but also with earlier baryon computations that addressed multiple spin nucleon resonances in search for parity doublets and are discussed in Table III.

The two (current) quark masses are near actual parameters in the QCD Lagrangian at 2 GeV, the reason being the implementation of spontaneous chiral symmetry breaking by a gap equation, unlike constituent quark models. The effective gluon mass present in the kernel in Eq. (36) was set to $m_g = 0.6$ GeV. Those parameters are fixed from the meson sector of the theory and yield around $m_\pi = 150$ MeV. Because spontaneous symmetry breaking is implemented, Goldstone's theorem and the Gell-Mann-Oakes-Renner relation are satisfied, so in the chiral limit $m_\pi = 0$; fine-tuning m_u easily yields the physical pion mass, but we see no point in reaching such a precision. As for the basic vector meson, with this set $m_{\rho/\omega} = 730$ MeV (about 40 MeV too low, but this resonance is 150 MeV broad, so this is not a big deal numerically). Finally, m_ϕ (a pure $s\bar{s}$ meson) has a mass

TABLE III. Parameters used in the model Hamiltonian and in the integration. The strange m_s is set at 70 MeV, but we also perform runs at 25 MeV to check the dependence thereof, and both are fixed in the gap function (momentum scheme) around 2 GeV, and m_g controls the kernels V, U of Eqs. (36) and (37), with the interpretation of a longitudinal gluon masslike parameter. The integral extends between an IR cutoff (to avoid an accidental divergence in the Monte Carlo with the IR-strong potential, but there is no dependence in it) and a UV cutoff to cover (most of) the corresponding variational wave function.

Hamiltonian parameters	
$m_u = m_d$	0.001 GeV
m_s	0.070 GeV
m_g	0.6 GeV

Integration controls	
λ_{IR}	3×10^{-3} GeV
Λ_{UV}	$\propto$ variational parameters

TABLE IV. Calibration computation of the $\Delta(1232)$ (all light quarks) and $\Omega^-(1672)$ (three strange quarks), with maximal spin $J = S = \frac{3}{2}$, $L = 0$. The Δ comes out 150 MeV heavier than the datum, in line with expectations for a pure qqq computation that does not incorporate its πN channel. Since it has a 130 MeV width, a positive 150 MeV deviation is very reasonable for this variational computation. Gell-Mann's Ω^- state, stable by the strong force, is calculated compatibly with its experimental mass. A few values around the minimum, rounded off to 5 MeV precision, are quoted.

	v_ρ (GeV)	v_λ (GeV)	$\langle H \rangle$ (GeV)
$\Delta(1232)$	0.3	0.4	**1.38 ± 0.04**
	0.4	0.4	1.46 ± 0.05
	0.4	0.3	1.45 ± 0.04
$\Omega(1672)$	0.4	0.4	**1.65 ± 0.04**
	0.4	0.3	1.73 ± 0.03
	0.5	0.3	1.69 ± 0.04
	0.5	0.4	1.72 ± 0.05

of 1030 MeV (again quite acceptable as its physical mass is 1020 MeV) for that value $m_s = 70$ MeV.

V. ESTIMATE OF SINGLET MASS IN THE NCSTATE COULOMB-GAUGE QCD MODEL: EXTENSIVE NUMERICAL COMPUTATIONS

In order to compute the mass of the $SU(3)$ flavor singlet, we have to evaluate the matrix elements of the Hamiltonian (presented in Sec. IV), with each of the selected families of variational wave functions. For that, the complete theoretical framework was implemented in a C++ program where the $\vec{k}_A$, $\vec{k}_B$, and $\vec{q}$ momentum integrals of Eq. (43) were estimated using the Monte Carlo-based multidimensional CUBA library [46]. Most frequently, we employed the well-known VEGAS algorithm therein [47], though we have also cross-checked with some of the other integration algorithms in the package.

The color Ward identities between the gap equation and the qqq kernel guarantee infrared finiteness [48,49] of the matrix element in Eq. (43) with the employed potential, that in the infrared $V \propto q^{-4+\epsilon}$ practically is the Fourier transform of a linear confining kernel. Still, the nine-dimensional momentum integral was regulated with an IR cutoff of 3×10^{-3} GeV to avoid any accidental apparent divergence, particularly in the exchanged momentum q in Eq. (43), due to the random distribution of points in the Monte Carlo algorithm. Additionally, for the Monte Carlo algorithm to correctly cover most of each variational wave function, an upper integration limit (Λ_{UV}) was introduced. As each wave function extends to different maximum momentum, this integration cutoff is scaled as a multiple of the (inverse) variational parameter. Therefore, it takes a different value in each of the computations, typically of order 3–10 times the relevant scale. For example, in

Sec. VA, the quoted values were obtained with $\Lambda_{\mathrm{UV}} = 5 \times \mathrm{MAX}(v_\rho, v_\lambda)$ as described therein.

That a small tail of the nominal wave function may extend outside the integration domain (and failed to be integrated over) does not cause a problem of principle: It amounts to a redefinition of the variational wave function as including an additional truncation parameter, so that it is multiplied by a step function. (There are smaller orthogonalization effects that need not concern us at the level of precision that the Monte Carlo evaluation achieves.) This is legitimate within the variational principle, as long as the same truncation of the integration is applied to the normalization so that $\frac{\langle \Lambda_S | \Lambda_S \rangle}{\langle 0 | 0 \rangle} = 1$. Therefore, we compute the normalization of the wave function with the same computer code and cutoffs, then use the obtained number to set it to 1. The variational approach is then sensible despite cutting off the integrations.

A. Computer code test: $\Delta(\frac{3}{2}^+)$ and $\Omega(\frac{3}{2}^+)$ baryons

Prior baryon computations in this scheme [50–52] focused on neutron-wave-function anisotropic deformation under the high compression of neutron stars and on parity doubling in the highly excited N/Δ spectrum.

As a renewed test of the computer code modified for this singlet hyperon application, the masses of two well-known baryons, Gell-Mann's decuplet $\Delta(1232)$ and $\Omega(1672)$, were computed first. These two baryons are archetypical qqq states with three light quarks (the Δ) and three strange quarks (the Ω) having particularly simple, completely symmetric qqq wave functions. We assume here perfect isospin symmetry so $m_u = m_d$. They are thus ideal cases to test the entire computer program (except, of course, the singlet wave function construction).

The parameters of these two Hamiltonian computations have been shown in Table III, and they are consistent with meson and earlier baryon work in the same model.

For this calibration exercise, variational wave functions were adapted from [50–52]. The radial wave function takes a rational form

$$R(k) = \frac{1}{\left[\left(\frac{|\mathbf{k}_\rho|}{v_\rho}\right)^4 + 1\right]\left[\left(\frac{|\mathbf{k}_\lambda|}{v_\lambda}\right)^4 + 1\right]} \tag{45}$$

with

$$\mathbf{k}_\rho := \frac{1}{\sqrt{2}}(\mathbf{k}_1 - \mathbf{k}_2),$$

$$\mathbf{k}_\lambda := \sqrt{\frac{3}{2}}(\mathbf{k}_1 + \mathbf{k}_2) \propto (\mathbf{k}_1 + \mathbf{k}_2 - 2\mathbf{k}_3) \tag{46}$$

appropriate Jacobi coordinates for the three-body problem in the center-of-momentum frame in which
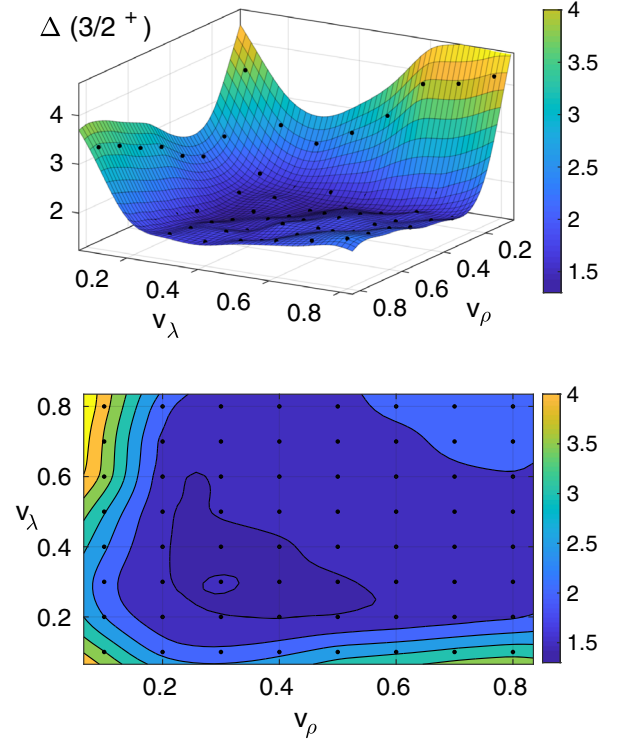

FIG. 7. $\langle H \rangle$ over the variational-parameter space of the $\Delta(1232)$ calibration test. The wave function (of rational form) is that of Eq. (45). The minimum energy obtained on the discrete grid is given in Table V. For visualization, a continuous surface is obtained from a biharmonic spline interpolation of the discrete values result of the MC simulations.

$$\mathbf{k}_1 + \mathbf{k}_2 + \mathbf{k}_3 = \mathbf{0}. \tag{47}$$

Each of their moduli is scaled by a corresponding v_ρ and v_λ variational parameter. This two-dimensional parameter space will later be scanned for a minimum of the variational mass, according to the Rayleigh-Ritz variational principle.

The variational-parameter spaces for the $\Delta(1232)$ and $\Omega(1672)$ are explored in Figs. 7 and 8, respectively. For each parameter pair in the two-dimensional grid, we obtained $\langle H \rangle(v_\rho, v_\lambda)$. After this calculation of E over the variational-parameter space grid, we extract its minimum that, by the variational principle, is an upper bound to the respective ground level energy. Those minima are carried over to Table IV.

The discrete values of E were continuously interpolated by a biharmonic spline for better visibility in the two figures. As is usual in these calculations, when the energy is known to precision ϵ, the wave function parameter is only obtainable to precision $\sqrt{\epsilon}$ (since the matrix element is quadratic in the wave function). Therefore, the minima present themselves as broad valleys depicted with the darkest shades in Figs. 7 and 8 (and following). In those dark areas, values of $\langle H \rangle$ under 2 GeV are found.
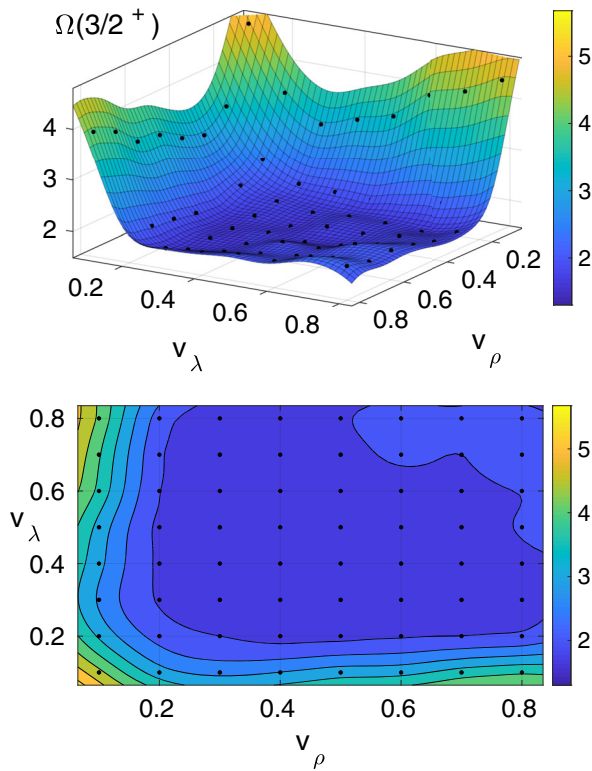
FIG. 8. $\langle H \rangle$ over the variational-parameter space of the $\Omega(1672)$ calibration test. The same wave function and methodology as in the $\Delta(1232)$ exercise of Fig. 7 was used. The minimum of $E(v_\rho, v_\lambda)$ over the discrete grid is given in Table V.

According to the Rayleigh-Ritz variational principle, all energies calculated are upper bounds to the physical particle mass within the given Hamiltonian, with the optimal one corresponding to the minimum of the variational surface. Nevertheless, due to the Monte Carlo computational method, down fluctuations can occur. Thus, we strove to increase the number of integration

TABLE V. Λ_S mass values around the minimum of each J^π state and hydrogenlike radial wave function [$R_n^{(0)}(k)$ *Ansatz*, Eq. (13)].

	Hydrogenlike *Ansatz* for Λ_S		
J^π	ρ_1 (GeV)	ρ_2 (GeV)	ρ_3 (GeV)	Mass (GeV)
---	---	---	---	---
$\frac{1}{2}^+$	0.6	0.8	1.1	2.7 ± 0.2
	0.6	0.8	1.2	2.7 ± 0.3
	0.6	0.8	1.3	2.8 ± 0.2
	0.6	0.8	1.4	2.6 ± 0.2
	0.6	1.0	1.0	2.8 ± 0.2
$\frac{3}{2}^-$	0.4	0.6	1.4	1.8 ± 0.2
	0.4	0.6	1.6	1.7 ± 0.2
	0.4	0.8	0.8	1.6 ± 0.3
$\frac{1}{2}^-$	0.4	0.4	1.4	1.9 ± 0.1
	0.4	0.4	1.6	1.8 ± 0.2
	0.4	0.6	0.6	2.0 ± 0.1

points until the number of fluctuations was small enough to keep the standard deviation at or below the 50 MeV level. The Monte Carlo uncertainty was reduced to this level as shown in Table IV (the uncertainty quoted there corresponds only to this Monte Carlo computation of the matrix element and not to the error induced by the variational principle, whose sign is known, but not its size).

The computer code was run at the modest group cluster of the theoretical physics department in Madrid and similar facilities.

The $\Omega(1672)$ computed energy is in fair agreement with the experimental value, indicating a correct implementation of the strange quark framework. The $\Delta(1232)$ comes out $\sim$150 MeV heavier than its physical mass, in line with expectations for a pure qqq computation that does not incorporate its πN channel. Since it has a 130 MeV width, a positive 150–200 MeV deviation is very reasonable for a variational computation.

From these calibration tests, we take the accuracy of the computations within the Coulomb-gauge Hamiltonian, including the Monte Carlo integration procedure, as
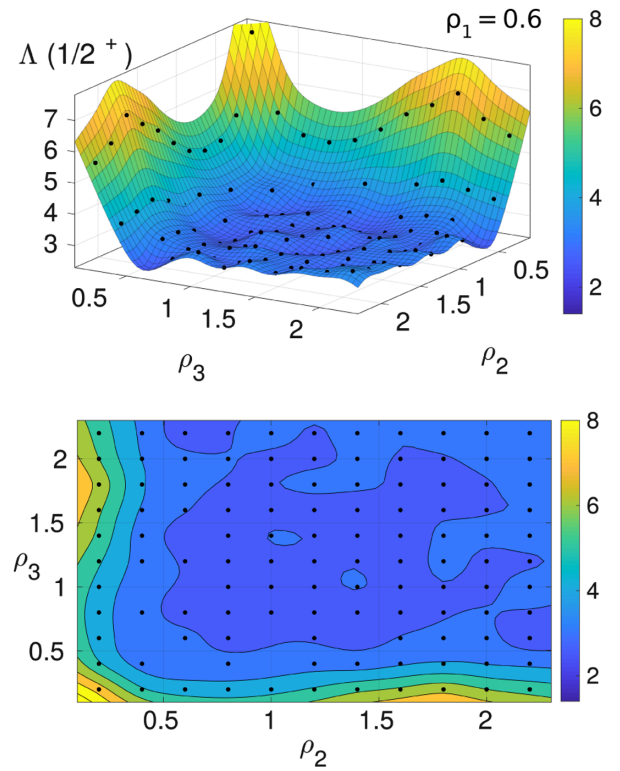

FIG. 9. $\langle H \rangle$ over the variational-parameter space for the $\Lambda(\frac{1}{2}^+)$ with hydrogenlike wave function $R^{(0)}$. The first variational parameter ρ_1 was fixed to 0.6 for which the lowest values where found. As in the calibration tests, the direct output of the Monte Carlo simulations was fitted to a continuous surface through a biharmonic spline interpolation. The minima providing the optimal upper bound for the energy of the baryon following the Rayleigh-Ritz principle are given in Table VI.
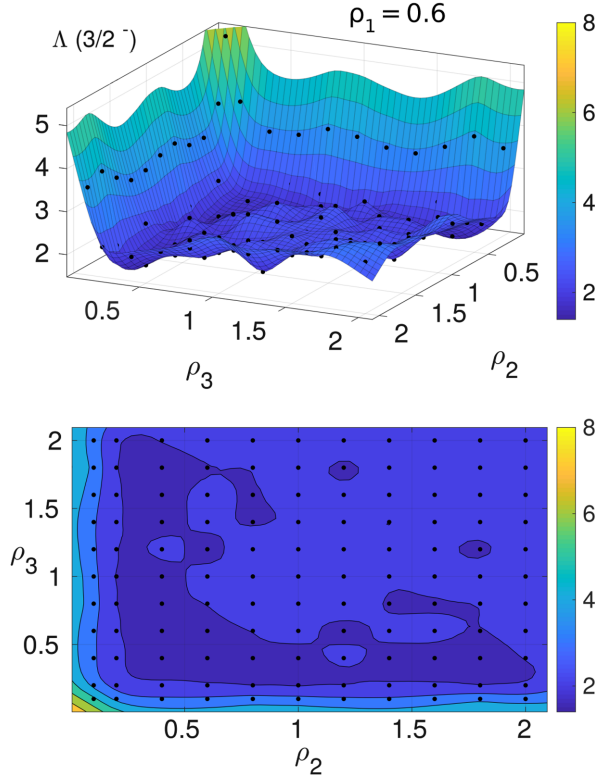
FIG. 10. Same as Fig. 9 for the $\Lambda(\frac{3}{2}^-)$ state, with hydrogenlike wave function $R^{(0)}$.
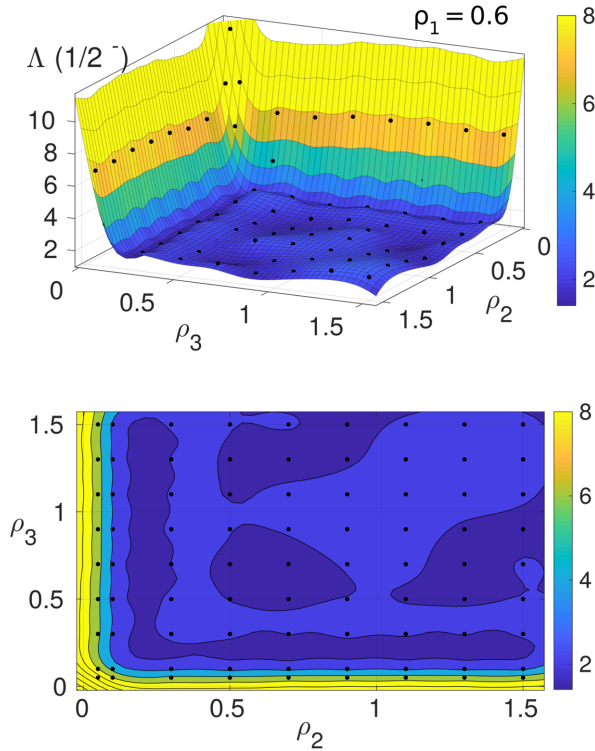

FIG. 11. Same as Fig. 9 for the $\Lambda(\frac{1}{2}^-)$ state with hydrogenlike variational wave function $R^{(0)}$.

validated, and reassert the adequacy of the Hamiltonian parameters used in past computations.

B. $\Lambda_S(qqq)$ flavor-singlet mass computation

We now proceed to the goal of this section. The only changes needed to determine the Λ_S states masses with the same Hamiltonian tested in Sec. V A concern the variational wave functions. Given the reasonable performance with the two tested single-flavor baryons in the decuplet, only a few modifications concerning the multiflavor structure had to be made.

Since their symmetry is more complicated, employing two variational parameters for the Jacobi variables k_ρ and k_λ turned out not to be the most straightforward procedure. Instead, the wave function was written down for each quark (guaranteeing the correct symmetry by applying appropriate symmetrization/antisymmetrization operators) so that three variational parameters had to be used. In comparing with the one-flavor cases, the mixed wave functions required a significantly large amount of computational time. To reduce it, we used the antisymmetry of the wave functions (explicitly tested in the code) to reduce the number of computed points in the variational space. This feature allowed us to speed the computation by a factor $\frac{N^N}{N!}$.

We have run the computer codes with all four radial *Ansätze* in Eq. (13) and following. The variational principle indicates that in each channel we should keep the minimum energy over each *Ansatz* family, and then in turn select the minimum among the four families. Figures 9–11 show $\langle H \rangle$ over the variational space for $R^{(0)}$, the variational wave function that is hydrogenlike, one figure for each J^π.

That hydrogenlike $R^{(0)}$ and also the $R^{(3)}$ based on an interpolation to the solution of the previously computed two-body problem, were generally superior to both of the harmonic oscillator (one- or three-dimensional) wave functions $R^{(1)}$ and $R^{(2)}$. For the $\frac{1}{2}^-$ and $\frac{3}{2}^-$, we quote results from the hydrogenlike $R^{(0)}$, that was as good as any (see Table V) and is of simple physical interpretation.

TABLE VI. Optimal variational estimate for the candidate singlet Λ_S mass in each J^π channel, and the wave function variational parameters that deliver it. Our somewhat unexpected finding is that the $\frac{1}{2}^+$ candidate is above 2 GeV.

	Minimum $\langle H \rangle_{\Lambda_S}$ with meson-derived *Ansatz* $R^{(3)}$			
J^π	ρ_1	ρ_2	ρ_3	E_0 (GeV)
$\frac{1}{2}^+$	2.5 ± 0.1	2.7 ± 0.1	3.1 ± 0.2	2.4 ± 0.2

	Minimum $\langle H \rangle_{\Lambda_S}$ with hydrogenlike *Ansatz* $R^{(0)}$			
J^π	ρ_1 (GeV)	ρ_2 (GeV)	ρ_3 (GeV)	E_0 (GeV)
$\frac{3}{2}^-$	0.4 ± 0.1	0.7 ± 0.1	1.2 ± 0.4	1.7 ± 0.2
$\frac{1}{2}^-$	0.4 ± 0.1	0.5 ± 0.1	1.0 ± 0.6	1.8 ± 0.2

For $\frac{1}{2}^+$ instead, the value of 2.7 GeV quoted in Table V, being a GeV above the singlets in the other channels, looks unnatural to us. In this case, we found the tabulated, interpolated, and rescaled $R^{(3)}$ to be optimal: The minimum of $\langle H \rangle$ drops by 0.3 GeV with respect to the hydrogenlike $R^{(0)}$ to yield the 2.4 GeV quoted in Table VI. That table collects the optimal value that we have been able to locate for each J^π combination and is the final result of this section.

VI. DISCUSSION

It seems to us that the qqq flavor singlets of lowest mass are well established to have quantum numbers $\frac{1}{2}^-$, $\frac{3}{2}^-$, and $\frac{1}{2}^+$, a result that we have rederived. Their masses are not too dissimilar in a harmonic oscillator picture of baryons (the two negative parity states would basically be degenerate, being in the first shell with $N = 1$ excitation in a non-relativistic setup and differing only in spin recoupling; the excitation energy of the positive parity state would be higher, jumping to the $N = 2$ shell with positive parity).

However, traditional flavor analysis [21] sometimes seems to ignore or do without the $\frac{1}{2}^+$ singlet, whose lowest mass candidate, $\Lambda(1810)$ as per the Graz effort [12], has recently been put into question [22] as unnecessary to explain scattering data. Experimentally reconfirming this state by different means then seems to be first-order business: We have shown in an explicit calculation of the relativistic, chiral-field-theory quark model extracted from Coulomb-gauge QCD, and respecting its global symmetries, that this $\frac{1}{2}^+$ singlet is heavier than the other two J^π channels, and well above 2 GeV.

This means that even after accounting for mixing and for the effect of the nucleon-meson decay channels, it is unlikely to be in agreement with a 1.8 GeV mass.

The negative parity candidates, on the other hand, appear in the 1.7–1.8 GeV range (with a 0.1–0.2 GeV Monte Carlo error), consistent with expectations based on other quark approaches.

The two experimental Λ candidates that could contain sizeable parts of this qqq singlet wave function configuration appear in the 1.4–1.6 GeV range. This is expected from $\Delta M \sim \Gamma$ relating the real and imaginary shifts of the particle pole upon including open baryon-meson channels, and from mixing with color octet configurations.

That the radial-like excitation is heavier than the angular ones is not surprising upon reexamining the meson spectrum: The $\rho(770)$ largely corresponds to the $q\bar{q}$ $(n_r = 1)^3 S_1$ state, the $(n_r = 1)^3 P_1$ corresponds to the $a_1(1260)$, and the $(n_r = 2)^3 S_1$ to the $\rho(1450)$. This entails the radial excitation to be 200 MeV above the orbital angular momentum one. A similar splitting separates the analogous $K_1(1270)$ and $K^*(1410)$.

In our baryon Λ_S computation, and after allowing for the Monte Carlo uncertainties, it appears that the splitting is a factor of 2 larger. Whether this is (a) an effect of the restriction to a flavor singlet, (b) a variational effect (that we have not gotten a variational wave function close enough to the true one for the Hamiltonian despite the four families with two independent parameters tried), (c) a model effect built into the Hamiltonian (despite its reasonable success in several other similar calculations), or (d) a true feature of QCD (and possibly of nature) remains to be seen, but we have detected no obvious error that makes us suspect of the result in Table VI.

If we were to dare a possible explanation, we would note the 150 MeV excess mass computed for the Δ baryon that can decay strongly; a similar effect should be there for these hyperon resonances, and one would broadly expect it to grow with the particle mass as more decay channels (ignored in a qqq calculation) would be open.

Even after such effects are discounted, the fact that qqq flavor-singlet baryon configurations have a mass so much larger than the ground-state baryon octet is a consequence of the color degree of freedom that forces them into an excited state. Additionally to the mass, the issue of baryon-singlet identification can profit from studying decay-product distributions. We have examined them with reasonable EFT-based hadron models and have shown how the branching fractions depend on the hyperon mass. In those decays, $SU(3)$ symmetry is more easily extracted from the data for decaying hyperons of higher mass: These see less pronounced effects of phase space and derivative couplings breaking $SU(3)$.

Because those effects are rather violent for low-lying resonances, we hope that symmetry analysis of decays will be more useful to screen the $M > 1.8$ GeV region for singlet candidates, where the experimental uncertainty can obfuscate the assignment much less.

Simultaneously, we hope to stimulate activity in lattice gauge theory toward untangling the octet-singlet $SU(3)$ flavor structure of the few low-lying resonances: It would be an interesting theoretical contribution to achieve such a separation.

ACKNOWLEDGMENTS

APPENDIX A: RARITA-SCHWINGER SPINORS AND $\Lambda_S(\frac{3}{2}^-)$ DECAY VERTEX

In this appendix, we give some detail on the calculation of the two-body $\overline{|\mathcal{M}|^2}_{\Lambda_S \to B\Phi}$ for the spin-parity $\frac{3}{2}^-$ combination.

Following [53], we take a collection of four spin-$\frac{1}{2}$ Dirac spinors grouped as the components of a Minkowski four-vector, $\psi_{RS\mu}$ or simply ψ_μ. Each of the spinors satisfies a free Dirac equation

$$(i\partial\!\!\!/ - M_{\Lambda_S})\psi_\mu(x) = 0, \tag{A1}$$

with $\partial_\mu \to -ip_\mu$ to convert to momentum eigenmodes.

Since ψ_ν is the tensor product of an object of spin-$\frac{1}{2}$ (each Dirac spinor) and one that contains spins 0 and 1 (the four-vector that collects them), this collection of spinors is not an irreducible representation of the rotation group (or of the Lorentz one, of course) and contains two spin-$\frac{1}{2}$ representations in addition to the $3/2$ of interest to the decay at hand.

One of the unwanted representations is removed by imposing the condition (see, for example, [54])

$$\gamma^\mu\psi_\mu = 0; \tag{A2}$$

as the four-vector index is contracted, this can be seen as a Dirac spinor condition. A second such condition can be obtained [55] by multiplying Eq. (A1) by γ^μ and using Eq. (A2) to simplify, yielding

$$\partial^\mu\psi_\mu = 0. \tag{A3}$$

This removes the second unwanted spin-$\frac{1}{2}$ representation, it being a condition in the $(0, 1/2)$ representation of the Lorentz group cover.

To proceed quickly to Γ_{Λ_S}, we need the positive-spinor completeness relation equivalent to the Dirac one,

$$\sum_\sigma u(\mathbf{p},\sigma)\bar{u}(\mathbf{p},\sigma) = \Lambda_+ = (p\!\!\!/ + M). \tag{A4}$$

This will be a certain tensor

$$\sum_\sigma u^\mu(\mathbf{p},\sigma)\bar{u}^\nu(\mathbf{p},\sigma) = \Lambda_+^{\mu\nu} = (p\!\!\!/ + M)(P^{3/2})^{\mu\nu} \tag{A5}$$

with the spin-$\frac{1}{2}$ parts projected out.

To construct the tensor following [56], let us first enforce Eq. (A3) by subtracting from the identity the projection over p_μ,

$$\eta_\perp^{\mu\nu} := \eta^{\mu\nu} - \frac{p^\mu p^\nu}{p^2}. \tag{A6}$$

The resulting spinor $\eta_\perp^{\mu\nu}\psi_\nu$ obviously satisfies $p_\mu\eta_\perp^{\mu\nu}\psi_\nu = 0$, and thus, Eq. (A3), and falls in the reducible $(1, 1/2)$ representation. It does not satisfy Eq. (A2), so we need to subtract another projection forming

$$(P^{3/2})^{\mu\nu} = \eta_\perp^{\mu\nu} - \frac{1}{3p^2}(p^\mu - \gamma^\mu p\!\!\!/)(p^\nu - p\!\!\!/\gamma^\nu). \tag{A7}$$

It is easy to check several properties: First,

$$\gamma_\mu(P^{3/2})^{\mu\nu} = 0 = p_\mu(P^{3/2})^{\mu\nu}, \tag{A8}$$

and $(P^{3/2})^{\mu\nu}\psi_\nu$ satisfies both Eqs. (A2) and (A3).

Second, $P^{3/2}(p)$ commutes with $p\!\!\!/$ so that it can be deployed to either side of $(p\!\!\!/ + M)$ in Eq. (A4). Third, it is indeed a projector

$$(P^{3/2})_\nu^\mu(P^{3/2})^{\nu\rho} = (P^{3/2})^{\mu\rho}, \tag{A9}$$

so that only one copy appears in Eq. (A4) that is constructed from two Rarita-Schwinger spinor collections.

Therefore, Eqs. (A4) and (A7) suffice to reconstruct Eq. (23) given the Lagrangian contribution yielding the decay.

It remains to construct this decay potential, for which we once more take into account that chiral symmetry requires in leading order that the meson be derivatively coupled. We also need to analyze the parity. The positive component of the RS spinor collection, after Fourier transform, is a sum, with some Clebsch-Gordan coefficients, of a Dirac spinor u multiplied by a spin-1 polarization vector ϵ_ν and with a particle creation operator $b^\dagger$, namely,

$$\psi_\nu^+ \propto \int \sum (\text{CG}) \cdot u \cdot \epsilon_\nu \cdot b^\dagger. \tag{A10}$$

The creation operator carries the intrinsic parity of the Λ_S particle $b^\dagger|0\rangle$, which is (-1) for the $\frac{3}{2}^-$ state, the spinor picks up a γ_0 in the Pauli-Dirac representation, and the vector ϵ_ν changes sign under parity. The γ_0 cancels out upon constructing a proper bilinear, so we count the RS field as having parity opposite to that of the particle.

Therefore, the parity-even effective vertex describing $\Lambda_S \to B\Phi$ is indeed that of Eq. (22).

APPENDIX B: INTEGRATION LIMITS IN THE DALITZ PLANE TO INTEGRATE THE THREE-BODY DECAYS $1 \to 2\,3\,4$

In this appendix, we quickly sketch the three-body formalism needed to carry out three-body decay calculations such as those in Sec. III C. The independent invariant Dalitz variables chosen are $m_{23}^2 \equiv p_{23}^2 \equiv (p_2 + p_3)^2$ and the analogous m_{24}. Energy-momentum conservation $p_1 = p_2 + p_3 + p_4$ entails that $\mathbf{p}_2$, $\mathbf{p}_3$, and $\mathbf{p}_4$ are coplanar in the cm system, where

$$m_{23}^2 = m_1^2 + m_4^2 - 2m_1 E_4 \tag{B1}$$

is rather simple, and once fixed,

$$m_{24}^2 = m_2^2 + m_4^2 + 2(E_2 E_4 - |\mathbf{p}_2||\mathbf{p}_4|\cos\theta_{24}). \quad \text{(B2)}$$

The border of the physical region in the (m_{23}, m_{24}) plane, the Dalitz plot, happens when the three-momenta are additionally collinear, $\cos\theta_{24} = 1$.

First, let us give the minimum values that the Dalitz variables can take; these are $m_{ij}^{\min} = m_i + m_j$, but they are not reached simultaneously. With a bit of work, inverting Eq. (B1) for E_4 (and equivalently for E_2, E_3) to retrieve $E_i^{\min}$, we obtain

$$m_{23}^2(m_{24}^{\min}) = m_1^2 + m_2^2 - \frac{m_2}{m_2+m_4}(m_1^2 - m_3^2 + (m_2+m_4)^2).$$
$$\text{(B3)}$$

Likewise, the maxima of each of the ij-Dalitz variables are reached when the remaining particle is left at rest, so that, for example,

$$m_{24}^{\max} = m_1 - m_3, \qquad E_3 = m_3. \quad \text{(B4)}$$

Some algebra leads, for example, to

$$E_4^{\max} = \frac{(m_1 - m_3)^2 + m_2^2 - m_4^2}{2(m_1 - m_3)} \quad \text{(B5)}$$

and

$$m_{23}^2(m_{42}^{\max}) = m_1^2 + m_4^2 - 2m_1 E_4$$
$$= m_4^2 + m_1 m_3 - m_1 \frac{m_4^2 - m_2^2}{m_1 - m_3}. \quad \text{(B6)}$$

The rest of the border can be obtained from the collinearity condition, the on-shell and momentum conservation conditions, yielding, for example,

$$E_4^{\pm} = \frac{1}{2m_{24}^2}\left[\frac{(m_{24}^2 + m_4^2 - m_2^2)(m_1^2 + m_{24}^2 - m_3^2)}{2m_1}\right.$$
$$\pm \sqrt{\left(\frac{m_1^2 + m_{24}^2 - m_3^2}{2m_1}\right)^2 - m_{24}^2}$$
$$\left. \times \sqrt{(m_{24}^2 + m_4^2 - m_2^2)^2 - 4m_{24}^2 m_4^2}\right] \quad \text{(B7)}$$

that can be substituted into

$$m_{23}^2(m_{24})_{\pm} = m_1^2 + m_4^2 - 2m_1 E_4^{\pm}(m_{24}^2) \quad \text{(B8)}$$

to complete the figure in the Dalitz plane. With the computed borders, the three-body widths are then straightforward to extract

$$\Gamma(m_1)|_{m_2,m_3,m_4} = \frac{1}{32(2\pi)^3 m_1^3}\int_{(m_{24}^{\min})^2}^{(m_{24}^{\max})^2} dm_{24}^2$$
$$\times \int_{m_{23}^2(m_{24})_+}^{m_{23}^2(m_{24})_-} dm_{23}^2 |\mathcal{M}(m_{23}^2, m_{24}^2)|^2. \quad \text{(B9)}$$

[1] M. L. Perl, E. R. Lee, and D. Loomba, Annu. Rev. Nucl. Part. Sci. **59**, 47 (2009).

[2] F. Bergsma *et al.* (CHARM Collaboration), Z. Phys. C **24**, 217 (1984).

[3] R. L. Delgado, C. Hidalgo-Duque, and F. J. Llanes-Estrada, Few-Body Syst. **54**, 1705 (2013).

[4] F. E. Close, *An Introduction to Quarks and Partons* (Academic Press, London, 1980), ISBN 012175152X.

[5] F. Halzen and A. D. Martin, *Quarks and Leptons: An Introductory Course in Modern Particle Physics*, 1st ed. (John Wiley & Sons, Hoboken NJ, 1984), ISBN 0471887412.

[6] C. Patrignani *et al.* (Particle Data Group), Chin. Phys. C **40**, 100001 (2016); P. A. Zyla *et al.* (Particle Data Group), Prog. Theor. Exp. Phys. (**2020**), 083C01.

[7] J. A. Oller and U. G. Meissner, Phys. Lett. B **500**, 263 (2001).

[8] D. Jido, J. A. Oller, E. Oset, A. Ramos, and U. G. Meissner, Nucl. Phys. **A725**, 181 (2003).

[9] U. G. Meiner, Symmetry **12**, 981 (2020).

[10] G. P. Engel *et al.*, Proc. Sci., Hadron2013 (**2013**) 118 [arXiv:1311.6579].

[11] J. M. M. Hall, W. Kamleh, D. B. Leinweber, B. J. Menadue, B. J. Owen, A. W. Thomas, and R. D. Young, Phys. Rev. Lett. **114**, 132002 (2015).

[12] T. Melde, W. Plessas, and B. Sengl, Phys. Rev. D **77**, 114002 (2008).

[13] H. W. Lin, Chin. J. Phys. **49**, 827 (2011).

[14] H. W. Lin, Nucl. Phys. B, Proc. Suppl. **187**, 200 (2009).

[15] M. Ronniger and B. C. Metsch, Eur. Phys. J. A **47**, 162 (2011).

[16] U. Löring, B. C. Metsch, and H. R. Petry, Eur. Phys. J. A **10**, 395 (2001).

[17] S. X. Qin, C. D. Roberts, and S. M. Schmidt, Few-Body Syst. **60**, 26 (2019).

[18] S. Meinel and G. Rendon, arXiv:2009.09313; Proc. Sci., LATTICE2016 (**2016**) 299 [arXiv:1608.08110].

[19] N. Nakajima, H. Matsufuru, Y. Nemoto, and H. Suganuma, AIP Conf. Proc. **594**, 349 (2001).

[20] P. Pauli (GlueX Collaboration) arXiv:1909.10877.

[21] V. Guzey and M. V. Polyakov, Ann. Phys. (New York) **13**, 673 (2004); arXiv:hep-ph/0512355.

[22] A. V. Sarantsev, M. Matveev, V. A. Nikonov, A. V. Anisovich, U. Thoma, and E. Klempt, Eur. Phys. J. A **55**, 180 (2019).

[23] K. Azizi, Y. Sarac, and H. Sundu, Phys. Rev. D **102**, 034007 (2020).

[24] D. Ebert, R. N. Faustov, and V. O. Galkin, Phys. Rev. D **84**, 014025 (2011).

[25] J. L. Rosner, J. Phys. G **34**, S127 (2007).

[26] S. K. Lin and W. Weise, Molecules **6**, 10411043 (2001); A. W. Thomas and W. Weise, *The Structure of the Nucleon* (Wiley-VCH, Berlin, 2001), ISBN .

[27] B. Ruijl, T. Ueda, and J. Vermaseren, arXiv:1707.06453.

[28] D. G. Robertson, E. S. Swanson, A. P. Szczepaniak, C.-R. Ji, and S. R. Cotanch, Phys. Rev. D **59**, 074019 (1999).

[29] F. J. Llanes-Estrada and S. R. Cotanch, Phys. Rev. Lett. **84**, 1102 (2000).

[30] A. P. Szczepaniak and E. S. Swanson, Phys. Rev. D **65**, 025012 (2001); A. Szczepaniak, E. S. Swanson, C. R. Ji, and S. R. Cotanch, Phys. Rev. Lett. **76**, 2011 (1996).

[31] E. Eichten, K. Gottfried, T. Kinoshita, K. D. Lane, and T. M. Yan, Phys. Rev. D **21**, 203 (1980).

[32] F. J. Llanes-Estrada, S. R. Cotanch, P. J. de A. Bicudo, J. E. F. T. Ribeiro, and A. Szczepaniak, Nucl. Phys. **A710**, 45 (2002).

[33] F. J. Llanes-Estrada, P. Bicudo, and S. R. Cotanch, Phys. Rev. Lett. **96**, 081601 (2006).

[34] F. J. Llanes-Estrada and S. R. Cotanch, Phys. Lett. B **504**, 15 (2001).

[35] I. J. General, F. J. Llanes-Estrada, and S. R. Cotanch, Eur. Phys. J. C **51**, 347 (2007).

[36] J. M. Torres-Rincon and F. J. Llanes-Estrada, Phys. Rev. Lett. **105**, 022003 (2010).

[37] P. Wang, S. R. Cotanch, and I. J. General, Eur. Phys. J. C **55**, 409 (2008).

[38] I. J. General, P. Wang, S. R. Cotanch, and F. J. Llanes-Estrada, Phys. Lett. B **653**, 216 (2007).

[39] L. M. Abreu, A. G. Favero, F. J. Llanes-Estrada, and A. García Sánchez, Phys. Rev. D **100**, 116012 (2019).

[40] L. M. Abreu, F. M. da Costa Júnior, and A. G. Favero, Phys. Rev. D **102**, 034002 (2020).

[41] L. M. Abreu, F. M. da Costa Júnior, and A. G. Favero, Phys. Rev. D **101**, 116016 (2020).

[42] See for recent work, see, e.g., R. Alkofer, C. S. Fischer, and H. Sanchis-Alepuz, EPJ Web Conf. **181**, 01013 (2018); Z. F. Cui, C. Chen, D. Binosi, F. De Soto, C. D. Roberts, J. Rodríguez-Quintero, S. M. Schmidt, and J. Segovia, Phys. Rev. D **102**, 014043 (2020).

[43] H. M. Choi and C.-R. Ji, Phys. Rev. D **95**, 056002 (2017).

[44] M. Gómez-Rocha, W. Schweiger, and O. Senekowitsch, Few-Body Syst. **55**, 697 (2014).

[45] F. J. Llanes-Estrada, S. R. Cotanch, A. P. Szczepaniak, and E. S. Swanson, Phys. Rev. C **70**, 035202 (2004).

[46] T. Hahn, Comput. Phys. Commun. **168**, 78 (2005).

[47] G. P. Lepage, Report No. CLNS-80/447, http://cds.cern.ch/record/123074.

[48] P. J. de A. Bicudo and J. E. F. T. Ribeiro, Phys. Rev. D **42**, 1625 (1990).

[49] A. Le Yaouanc, L. Oliver, S. Ono, O. Pène, and J.-C. Raynal, Phys. Rev. D **31**, 137 (1985).

[50] P. Bicudo, M. Cardoso, T. Van Cauteren, and Felipe J. Llanes-Estrada, Phys. Rev. Lett. **103**, 092003 (2009).

[51] P. Bicudo, M. Cardoso, F. J. Llanes-Estrada, and T. Van Cauteren, Phys. Rev. D **94**, 054006 (2016).

[52] F. J. Llanes-Estrada and G. M. Navarro, Mod. Phys. Lett. A **27**, 1250033 (2012).

[53] W. Rarita and J. Schwinger, Phys. Rev. **60**, 61 (1941).

[54] T. R. Hemmert, B. R. Holstein, and J. Kambor, J. Phys. G **24**, 1831 (1998).

[55] F. J. Milford, Phys. Rev. **98**, 1488 (1955).

[56] H. M. Siahaan, M.S. thesis, Technological Institute of Bandung, 2008, http://www.fisikanet.lipi.go.id/data/1014224401/data/1202810210.pdf.